INCLUSION OF CELECOXIB IN SBA-15 MESOPOROUS SILICA: DRUG
LOADING AND RELEASE PROPERTY

A THESIS SUBMITTED TO

THE GRADUATE SCHOOL OF NATURAL AND APPLIED SCIENCES

OF

MIDDLE EAST TECHNICAL UNIVERSITY

BY

ZEYNEP SEDA EREN

IN PARTIAL FULFILLMENT OF THE REQUIREMENTS

FOR

THE DEGREE OF MASTER OF SCIENCE

IN

CHEMISTRY

2016

Approval of the thesis:

INCLUSION OF CELECOXIB IN SBA-15 MESOPOROUS SILICA: DRUG LOADING AND RELEASE PROPERTY

submitted by **ZEYNEP SEDA EREN** in partial fulfillment of the requirements for the degree of **Master of Science in Chemistry Department, Middle East Technical University** by,

Prof. Dr. Gülbin Dural Ünver
Dean, Graduate School of **Natural and Applied Sciences** _____

Prof. Dr. Cihangir Tanyeli
Head of Department, **Chemistry** _____

Prof. Dr. Ayşen Yılmaz
Supervisor, **Chemistry Department, METU** _____

Examining Committee Members:

Prof. Dr. Şeniz Özalp Yalman
Chemical Eng. and Applied Chemistry Dept., Atılım Uni. _____

Prof. Dr. Ayşen Yılmaz
Chemistry Dept., METU _____

Assoc. Prof. Dr. Gülay Ertaş
Chemistry Dept., METU _____

Assoc. Prof. Dr. Sreeparna Banerjee
Biology Dept., METU _____

Assoc. Prof. Dr. Emren Nalbant Esentürk
Chemistry Dept., METU _____

Date: 01.08.2016

I hereby declare that all information in this document has been obtained and presented in accordance with academic rules and ethical conduct. I also declare that, as required by these rules and conduct, I have fully cited and referenced all material and results that are not original to this work.

Name, Last name: Zeynep Seda Eren

Signature:

ABSTRACT

INCLUSION OF CELECOXIB IN THE SBA-15 MESOPOROUS SILICA: DRUG
LOADING AND RELEASE PROPERTY

Eren, Zeynep Seda

M. Sc., Department of Chemistry

Supervisor: Prof. Dr. Ayşen Yılmaz

2016, 64 pages

Mesoporous silica particles have been used to enhance the loading capacity of drugs
into the support, increase the solubility of drug and control drug release.

In this study, poorly water-soluble, nonsteroidal anti-inflammatory drug with rela-
tively low bioavailability Celecoxib, was used as a model drug in order to determine
the drug loading and release properties of silica particles. In order to synthesize SBA-
15 particles, hydrothermal synthesis method was used, SBA-15 samples were func-
tionalized by post-grafting method with (3-Aminopropyl) triethoxysilane, APTES
(SBA-15-A). Moreover, Boron doped SBA-15 (SBA-15-B) samples were prepared
and borosilicate samples were obtained. After APTES functionalization and Boron
doping process, drug was loaded to the particles in three different solvents; ethanol,
methanol and hexane to observe the effect on drug loading and release properties.

Particle morphology and solvent effect on drug loading capacity of the silica particles
were investigated and the effect of pH on drug release was studied. For this purpose,

SBA-15 particles were characterized by using x-ray diffraction (XRD), small – angle x-ray spectrometry (SAXS), N_2 adsorption - desorption, Fourier transform infra-red spectroscopy (FT-IR), differential scanning calorimetry (DSC), scanning electron microscope (SEM), transmission electron microscope (TEM), ultraviolet-visible spectrometry (UV-vis) and thermogravimetric analysis (TGA).

Then, highly improved release rate of Celecoxib by using SBA-15 silica particles as drug carriers compared with the commercial drug, Celebrex. For the release experiments of the Celecoxib particles in all silica samples, phosphate buffer solution (PBS) was used in pH=7.4 and pH=5 at 37 ˚C. According to release results, slow release for SBA-15-A (APTES functionalized SBA-15) particles was observed, while there was burst release for SBA-15-B (Boron doped SBA-15) particles and all silica samples prepared by hexane solvent.

All of the results demonstrated here confirm the potential use of silica supports as potential drug delivery carriers for poorly water soluble drugs.

Keywords: SBA-15 particles, surface functionalization, borosilicate, drug delivery systems, Celecoxib.

ÖZ

SBA-15 MEZOGÖZENEKLİ SİLİKA PARÇACIKLARINA SELEKOKSİB YÜKLEME ÇALIŞMALARI: İLAÇ YÜKLEME VE BIRAKMA ÖZELLİKLERİ

Eren, Zeynep Seda

Yüksek Lisans, Kimya Bölümü

Tez Yöneticisi: Prof. Dr. Ayşen Yılmaz

2016, 64 sayfa

Mezogözenekli silika parçacıkları, ilaçların yüklenme kapasitelerini artırmak, ilacın sudaki çözünürlüğü arttırmak ve ilaç salınımı kontrol etmek için kullanılmaktadırlar.

Bu çalışmada, suda az çözünen, steroid yapıda olmayan iltihap önleyici ve düşük biyoyararlanıma sahip Selekoksib, silica parçacıklarının yüklenme ve salınım özelliklerini belirlemek amacıyla model ilaç olarak kullanılmıştır. SBA-15 parçacıklarını sentezlemek için, hidrotermal sentez metodu kullanılmıştır ve SBA-15 örneklerinin yüzeyi (3-Aminopropil trietoksisilan) APTES ile post-grafting metoduyla fonksiyonlanmıştır ve SBA-15-A örnekleri elde edilmiştir. Daha sonra Bor katkılanmış SBA-15 örnekleri hazırlanmış ve borosilikat parçacıkları, SBA-15-B elde edilmiştir. APTES fonksiyonlanması ve Bor katkılanması işlemlerinden sonra, yüklenme ve salınım özelliklerinin etkisini incelemek için üç farklı çözücüde etanol, methanol ve hekzan içinde ilaç yükleme yapılmıştır.

Parçacık morfolojisi ve çözücünün silika parçacıklarının ilaç yükleme kapasitesi üzerindeki etkileri araştırılmış ve pH'ın ilaç salınımı üzerindeki etkisi analiz edilmiştir. Bu amaçla, SBA-15 parçacıklarının karakterizasyonu X-Işınları toz kırınımı (XRD),

küçük-açı x-ışınları saçılması (SAXS), N_2 adsorpsiyon-desorpsiyon, Fourier-transform kızılötesi spektroskopi (FT-IR), diferansiyel taramalı kalorimetre (DSC), taramalı elektron mikroskobu (SEM), geçirimli elektron mikroskobu (TEM), ultraviyole görünür bölge spektroskopi (UV-vis) ve termo gravimetrik analiz (TGA) yöntemleri kullanılarak yapılmıştır.

İlaç taşıyıcı olarak kullanılan SBA-15 silika parçacıkları, ticari ilaç olarak kullanılan Celebrex ile karşılaştırıldığında Selekoksib'in salınım oranını arttırmıştır. Silika örneklerindeki Selekoksib parçacıklarının salınım deneyleri için fosfat tampon çözeltisi (PBS) 37 ˚C'de pH=7.4 ve pH=5.0'da kullanılmıştır. Salınım sonuçlarına göre, SBA-15-A (APTES fonksiyonlanmış SBA-15) parçacıkları yavaş bir salınım gösterirken, hekzan çözücüsünde hazırlanmış SBA-15-B (Bor katkılanmış SBA-15) parçacıklarının salınımı hızlı olmuştur.

Elde edilen tüm sonuçlar suda çözünürlüğü az olan ilaçlar için silika taşıyıcıların potansiyel kullanımını doğrulamaktadır.

Anahtar Sözcükler: SBA-15, yüzey fonksiyonlama, borosilikat, kontrollü ilaç taşıma sistemleri, Selekoksib.

To my family ..

ACKNOWLEDGEMENT

TABLE OF CONTENTS

LIST OF TABLES

TABLES

LIST OF FIGURES

FIGURES

LIST OF ABBREVATIONS

APTES: Aminopropyltriethoxysilane

BET: Brunauer-Emmett-Teller

BJH: Barret-Joyner-Halenda

COX: Cyclooxygenase

d: the distance between adjacent crystal planes

DDS: Drug Delivery System

FT-IR: Fourier Transform Infra-red Spectroscopy

GI: Gastrointestinal tract

MCM: Mobil Composition Matter

NSAID: Non-steroidal anti-inflammatory drug

PBS: Phosphate Buffer Solution

SAXS: Small-Angle X-Ray Scattering

SBA: Santa Barbara Amorphous

SBA-15@Clx: Celecoxib loaded SBA-15 sample

SBA-15-A: amine functionalized SBA-15

SBA-15-A@Clx: Celecoxib loaded amine functionalized SBA-15 sample

SBA-15-B: boron doped SBA-15

SBA-15-B@Clx: Celecoxib loaded boron doped SBA-15 sample

SEM: Scanning Electron Microscopy

TEM: Transmission Electron Microscopy

TEOS: Tetraethylorthosilicate

UV: Ultra Violet

XRD: X-Ray Diffraction

CHAPTER 1

1. INTRODUCTION

The ability of interactions between porous materials and atoms, ions, molecules or nanoparticles has gained great attention since 1990s. Manipulation and design of pores in nanoparticles have increased for different science and technological purposes in modern society. Porous materials were classified into microporous (with pore diameter smaller than 2 nm), mesoporous (with pore diameter between 2 nm and 50 nm), and macroporous (with pore diameter larger than 50 nm) [1].

Nanoparticles as drug delivery devices can include various materials such as polymers, lipids and ceramics. With the advance of nanoparticles and drug carriers, efficient treatment of many cancer diseases could be achieved [2].

1.1 MESOPOROUS MATERIALS

Mesoporous materials (MSNs) were firstly synthesized in the 1990s and their applications were extensively used in separation, catalysis, sensors, adsorption, enzyme immobilization and devices. They are ideal for drug delivery systems as carriers due to their highly ordered structures, larger surface areas and pore sizes, good compatibilities with other materials. According to the article published by Liu J. et al. in 2013, various porous sizes, different functionality of mesoporous materials may be important factors influencing the drug loading and release kinetics [2].

The main effort carried out by scientists in the early 2000s is to improve mesoporous materials as an excellent candidate for cell-specific delivery. MSNs are synthesized in two ways; the first one includes condensation of silica under a basic medium with a cationic agent. The second approach is to use not only cationic agents, but also anionic and non-ionic surfactants [3]. MSNs have modifiable pore structure, stable rigid

framework and pore diameter is in range between 2-20 nm. Besides unmodified surfaces of MSNs show less controllable drug release due to weak interactions between drug and unmodified surfaces [4].

1.1 TYPES OF MESOPOROUS MATERIALS

1.1.1 SBA

Santa Barbara Amorphous (SBA) materials were firstly synthesized in 1998 [5]. Pore diameters of SBA range from 5 nm to 30 nm depending on the polymer type and reaction conditions. There are many types of SBA materials like SBA, SBA-16, SBA-15, SBA-14 and SBA-11. The most synthesized and searched SBA type is SBA-15 [6].

1.1.1.1 SBA-15

Large and controlled pore size, highly ordered hexagonal structure make SBA-15 the most preferable choice for catalysis, mainly drug delivery systems. Synthetic conditions of SBA-15 synthesis may change its morphology, for example; pore size varies 4-30 nm. SBA-15 forms weak intermolecular H bonding.and SBA-15 has very good hydrothermal stability. It is very attractive for surface modification [7, 8]. Ordered mesoporous silica, SBA-15, is presented in the Figure 1.
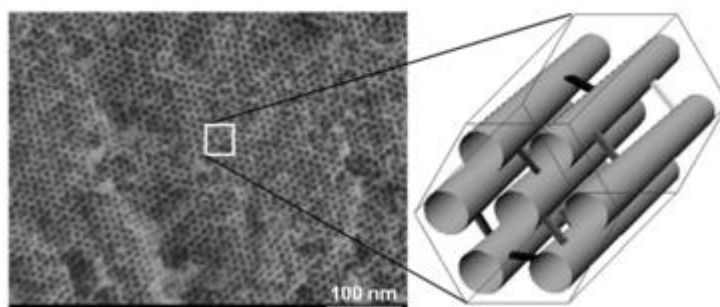
Figure 1 Representation of pore arrangement of ordered SBA-15 silica material [9].

1.1.2 M41S

In 1991, the scientists were not looking for mesoporous materials, however they developed a procedure mixing ammonia, tetramethylammonium silicate and the surfactant cetyltrimethylammonium bromide and patented [8]. These type of materials were named in the class of M41S. M41S materials synthesis made an improvement on the

newly synthesized zeolites, single molecules or cations which are used as templates for the mesoporous materials synthesis. Different organic materials addition and variable reaction conditions (temperature, pH, crystallization time, pressure, etc.) can control the structure of mesoporous material [8]. There are three types of M41S in MCM (Mobil Composition of Matter) group; cubic MCM-48, hexagonal MCM-41 and lamellar MCM-50.

1.1.2.1 MCM-48

MCM-48 has cubic pore system. Mass transfer kinetics was provided by regular pore network of MCM-48 and it is more favorable material than MCM-41 for catalytic and seperation technologies [10]. Figure 2 shows the cubic cell of pore MCM-48.
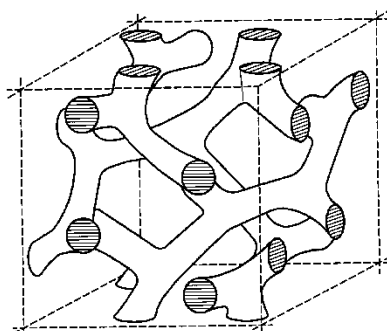
Figure 2 Cubic unit cell of pore MCM-48 [11].

1.1.2.2 MCM-41

When sodium silicate solution is added $C_{16}H_{33}$ $(CH_3)_3NOH/Cl$ surfactant, the earliest MCM-41 is synthesized. MCM-41 has nearly 4.0 nm as well as hexagonal array of uniform mesopores [12]. Figure presents the structure of MCM-41 and MCM-50 mesoporous silica. Pore length of MCM-41 is greater than its pore diameter and pore networking effects are negligible small. The pore walls of MCM-41 are made of tetrahedral silica arrangement, so the interconnections between pores are not energetically favorable [13].
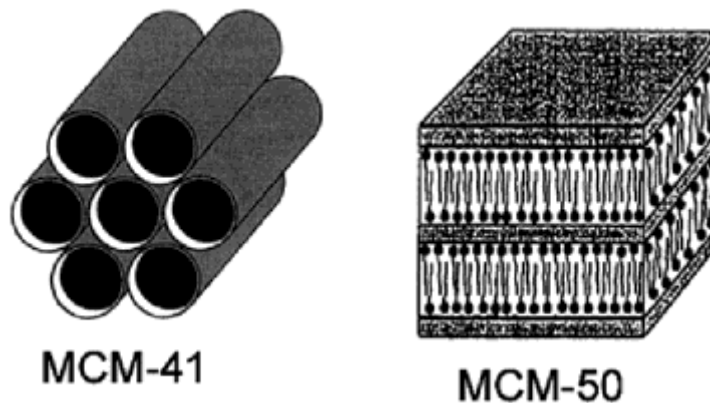
Figure 3 Representation of MCM-41 and MCM-50 [14].

1.1.2.3 MCM-50

MCM-50 is the second synthesized mesoporous material among M41S family. It has lamellar structure and thick pore walls as well as it shows low stability. Because of MCM-50's hard and long timed synthesis method, scientists had less attention to this mesoporous silica [15].

1.2 APPLICATIONS OF MSNs

During the last two decades, nanoscale materials have started to be used in different application areas. Firstly, mesoporous materials have been attracted by scientists in technical sciences such as catalysis, electronics, photocatalytic hydrogen production, solar cells, and battery components [16].

One of the most important mesoporous materials is mesoporous silica. Since the improvement of M41S mesoporous silica, large amount of research have been conducted on the biomedical science and medicine, specifically drug delivery systems, tissue engineering, drug targeting, and gene transfection. In Figure 14, it is seen the whole application areas of mesoporous silica which mainly focuses diagnostics, engineering and drug targeting systems. Because of excellent properties of mesoporous silica like hydrothermal stability, well biodegradability and biocompatibility, they are studied mainly for biotechnological purposes. Moreover, they offer an advantage for biologic applications, because mesoporous silicates have low toxic nature. Mesoporous silica samples are highly useful for drug delivery systems, because they include ordered pore

arrangement, high pore volume, large specific surface area and surface functionalization chance. Tamanoi, Mei, and their co-workers reported that they have synthesized promising anti-cancer drug carriers depending on pH and modification. [17]. Effective nanoscale drug carriers were improved with new synthesis and design methods for patience compliance and decreased adverse side effects. [4].
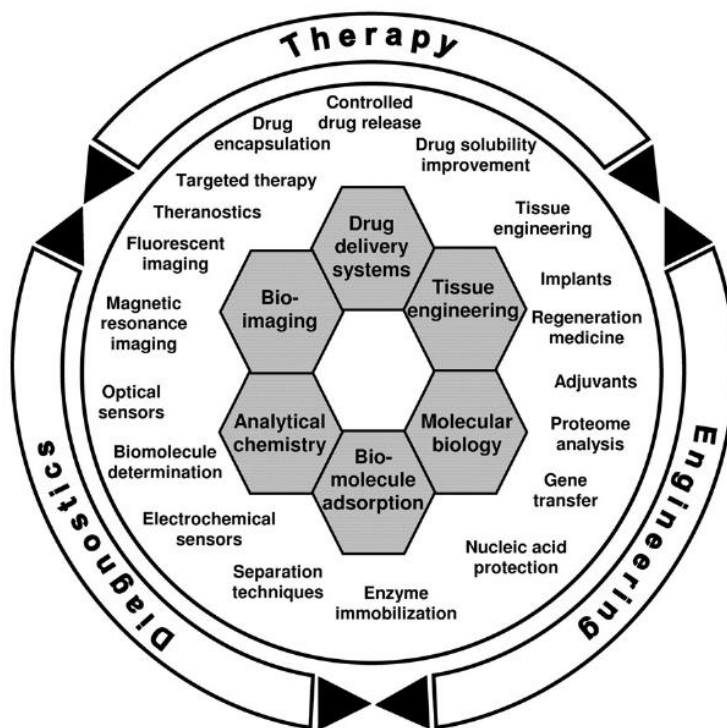
Figure 4 Application areas of mesoporous silica material [17].

1.3 SURFACE FUNCTIONALIZATION

Mesoporous materials have an advantage for easy functionalization with variable organic moieties in different parts of the particle; therefore, specialized tasks are enabled. One of the most important way of modifying chemical properties and physical characteristics of mesoporous silica would be done with modifying the surface of silica with organic and inorganic components. Surface functionalization comprises two different types; first one is one pot synthesis and second one is post-grafting.

1.3.1 ONE-POT SYNTHESIS (CO-CONDENSATION)

The one-pot type of synthesis involves a reaction of three or more compounds in a single vessel. The efficiency of the reactants increases, because more than one step is

formed in same reaction conditions without isolation of intermediates. There are various advantages of these type of reactions such as high acceleration, effectiveness, desired ranges and eco-friendly. Moreover, the synthesis of drug like heterocyclic compounds are obtained from this method [18].

Surface functionalization of silica particles in one pot synthesis is done with alkoxysilanes/halosilanes [19]. Alkoxysilanes will bind Si-O-Si groups to the surface, however halosilanes will hydrolize for alcohol groups in order to form Si-O-Si links with surface silanol groups. Surface silanol groups will react directly with halosilanes for anhydrous conditions. 3-aminopropyl triethoxysilane (APTES), 3-mercaptopropyl trimethoxysilane (MPTS) and various PEG-silanes are the most commonly used functional groups Functional groups are evenly distributed throughout the entire material when the substituted groups are electrostatically compatible with the surfactant [19, 20].

1.3.2 POST-GRAFTING

Post-grafting synthesis is used to modify pre-fabricated inorganic mesoporous material surface by attachment of functional groups to the surface material after surfactant removal. In the post-grafting synthesis method, silica surface is modified with organic moieties. The difference between post-grafting and co-condensation method was approved by Lim and Stein while performing nitrogen adsorption experiments, X-ray photo-electron microscopy and reaction kinetics. They noticed that in post grafting method, substituted group was dispersed heterogeneously in mesoporous silica and they were located on the external surface [21].

One of the most important advantage of this synthesis is to obtain ordered mesoporous material after the process. Secondly, a wide variety of functionalization group can be used according to the compatibility and hydrothermal stability is increased when compared to co-condensation. General reaction conditions consist of 24 hour reflux in a non-polar solvent in the presence of organosilanes [22].

Boron trioxide could also be added to silica mesoporous materials for functionalization process, so thermal capability and chemical resistance is increased. Boron doped material is used for conductors, optical devices, biomedical fields; especially drug delivery area [23].

CHAPTER 2

2. CONTROLLED DRUG DELIVERY SYSTEMS

Drug delivery systems (DDSs) are designed to change pharmacokinetics and pharmacodynamics of drugs, which are approved by Food and Drug Administration [24]. New drug molecule development is very expensive and takes too much time for further steps. The efficiency ratio of commercial drugs was improved with various techniques like drug therapy, dose titration and drug monitoring. Drug delivery controls the rate in an effective way and targeted delivery has been interested by researches for a few decade [25]. DDSs affect the pharmacokinetic profile of the drug, drug release rate, drug side-effects and drug release duration. An optimal DDS involves correct time and duration drug release. Drug concentration should be below minimal toxic concentration (MTC) and above minimal effective concentration (MEC). This concentration range is called therapeutic range. Though there are various drug administration routes like nasal, ocular, transdermal, pulmonary and parenteral; the most convenient route for drug delivery is oral delivery [26]. Controlled DDSs are leading to the applications for biomedical materials and new therapeutic agents. Drug delivery systems involve many different types. The aim of these systems is the same; however they benefit from various carriers and drug molecules. Ideal drug carriers such as polymers, liposomes should be non-toxic, biocompatible, biodegradable and stable. The mechanized silica nanoparticles are mainly the vehicles for drug delivery systems [27]. Commercial DDSs use polymer based technology which is very successful in these areas. However, the main problem of DDS is the decrease in drug activity until it reaches the target tissue [28].
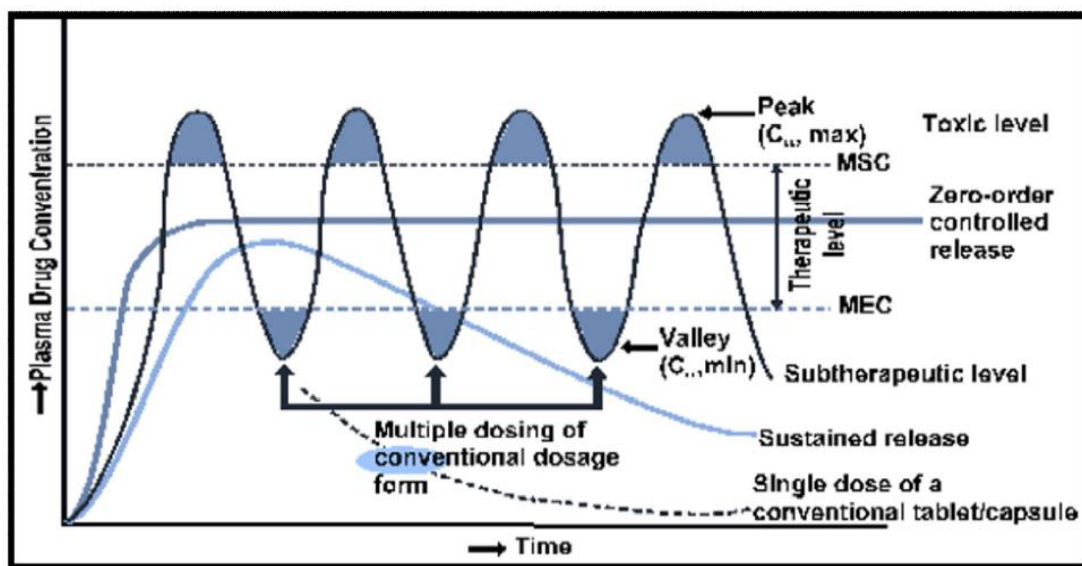
Figure 5 A hypothetical plasma concentration-time profile from conventional multiple dosing and single doses of sustained and controlled delivery formulations [28].

These days, a lot of research studies consisting of the mesoporous silica usage for drug design have been done. There are many textural properties of mesoporous silica that influence the performance of DDSs. Firstly, pore size is one of the factor controlling the drug release rate. Andersson et al. reported that geometry, pore connectivity, matrix degradation are also drug release controllers. Secondly, adsorptive properties of mesoporous materials, especially surface area is responsible from drug loading process. Higher or lower doses of pharmaceuticals can be determined by available surface area amount. Thirdly, pore volume is important for the amount of drug adsorbed, hence larger filling of mesopores is related to increased drug amount. Furthermore, functionalization could be attributed to the drug-surface interaction, the process controls drug adsorption and release. To increase drug-surface interaction and to reach effectively controlled release, chemical groups are linked to the surface. Song et al. reported that amine functionalized MCM-41 and SBA-15 mesoporous silica based materials control the Ibuprofen release through ionic bonds and ester bonds [30, 31].

10

CHAPTER 3

3. HYDROPHOBIC DRUGS

Oral drug administration route is the most common and preferred method for delivery because of its feasibility and convenience; however the problem is poor drug solubility or poor membrane penetrability. Drugs are mostly orally taken. In order to reach desired concentration of them in the system, scientists have been researched on biopharmaceutical properties of drugs [32]. Heterogenous molecules which have poor solubility in water, but higher solubility in organic solvents are called "hydrophobic drugs". Generally, these kind of molecules are divided into three, slightly soluble (1-10 mg/ml), very slightly soluble (0.1-1 mg/ml) and insoluble (<0.1 mg/ml) molecules [33] More than 40% drugs are identified as poorly water soluble. Because of low solubility and dissolution, the bioavailability of drugs is limited [34]. First pass metabolism, stability, transport, solubility and dissolution influence the bioavailability of orally taken drugs. Poorly water soluble compounds mostly are not dissolved and absorbed in blood; so they are not eliminated from the GI tract [35].

Process of Solubilization:

Solubilization process includes intermolecular and inter-ionic bonds breaking, separation of solvent or solute molecules and interaction between them. The process has three steps; firstly holes of solvent open. Secondly, solid molecules breaks away from the bulk. Lastly, free solid particles are included in the solvent. The solubility is related to solvent composition and physical properties of the system such as polarity of materials and molecular size of solvent. When the solid particle size is decreased, surface area of the particle increases; so solubility will enhance with a greater interaction. Moreover, high temperature increases the solubility of a drug due to absorbed energy. Pressure change mainly does not affect the solubility. Besides, molecules having higher molecular weight, solubility tends to decrease for a substance [36].

11
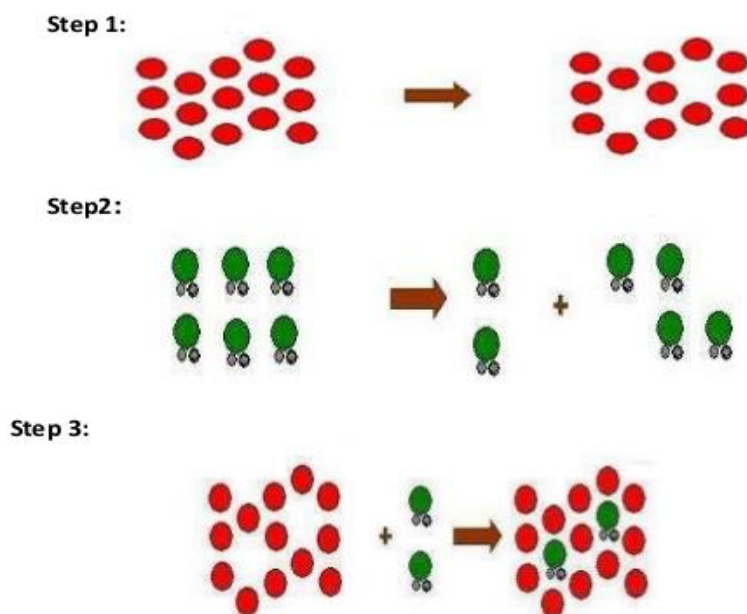
Figure 6 Mechanism of solubilization [36].

Salt formation and particle size reduction help to increase solubility and bioavailability of drugs by oral absorption though the practical limitations. It is not easy to form salt compounds, because weakly basic or acidic salt formations may not be feasible for neutral compounds. Although the solubility is increased by salt formation, reconversion of salts in GI tract may create a problem. In 1961, Sekiguchi and Obi created solid dispersion method in order to overcome low solubility and bioavailability of drugs. In solid dispersion method, the drug is dispersed an inert matrix at solid state mixture prepared by the melting of ingredients. When solid dispersion is dissolved in the medium, drug is released as colloidal particles. Increased surface area is expected to be high in dissolution rate and bioavailability of drug. On the other hand, preparation technique, reproducibility, dosage, the formulation and chemical stability of drug may limit the commercial application of this method [37, 38].

Attempts to overcome difficulties in solubility of poorly soluble drugs have been improved with changing their parental formulation. Changing solute or solvent properties may increase the solubility of drugs. According to Yalkowsky; buffers, surfactants and complexing agents can increase the solubility of a nonpolar drug. [39] Reducing the

hydrophobic particle size by using Ostwald-Freundlich equation is an efficient way for increase bioavalibility and solubility. However, drug loaded amount is decreased dramatically, it is reported in 2013 that loading amount is reached maximum by optimizing the particle size. [40].

3.1 CELECOXIB AND ITS PHARMACOLOGY

Celecoxib which is a nonsteroidal anti-inflammatory drug (NSAID), is approved for use as a pain killer (an analgesic). Celecoxib is 4-[5-(4-Methylphenyl)-3-(trifluorome-thyl)-1H-pyrazol-1-yl] benzenesulfonamide. The empirical formula of Celecoxib is $C_{17}H_{14}F_3N_7O_2S$, and its molecular weight is 381.37. Celecoxib has anti-inflammatory properties as well as antipyretic activities; this agent inhibits cycloxygenase (COX) enzyme. There are mainly two COX enzymes which are COX-1 and COX-2. COX-1 and COX-2 have dissimilar expression patterns in the tissues, COX-1 has functions in GI cytoprotection and vascular homeostasis. On the other hand, COX-2 induces inflammation. Generally, NSAIDS are not selective for COX enzymes which are involved in the synthesis of prostaglandin enzyme. Celecoxib inhibits selectively COX-2 enzyme. Epidemiological studies show Celecoxib can be used in the future as an anticancer drug since non-steroidal inflammatory drugs like Celecoxib have an effect on decreased the risk of colon cancer [41, 42].
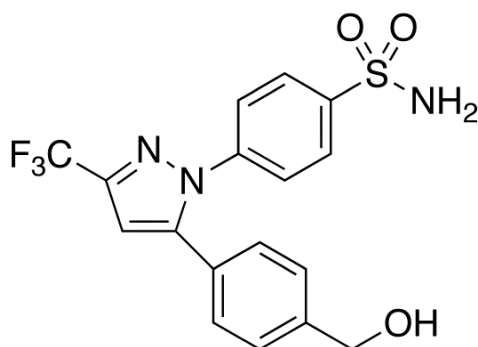
Figure 7 Structure of Celecoxib, 4-[5-(4-methylphenyl)-3-trifluoromethyl)-1H-pyra-zol-1-yl] benzene sulfonamide [43].

3.2 AIM OF THE WORK

In this thesis, the first aim is to prepare SBA-15, SBA-15-A (amine functionalized SBA-15) [44] and SBA-15-B (boron doped SBA-15) silica particles with using doping

13

and functionalization techniques. Hydrophobic drug, Celecoxib was chosen for model drug for drug loading and release processes. Morphology and solvent effect on drug loading amount of the silica particles were investigated and the pH effect on drug release was compared for three different Celecoxib loaded silica particles in ethanol, methanol and hexane. To analyze the effects of surface functionalization and boron doping, amine functionalized silica particles (SBA-15-A) and boron added silica particles (SBA-15-B) were prepared. Drug loading and release behavior of empty SBA-15, functionalized and doped SBA-15 particles were compared. At pH=5.0 and pH=7.4, the release trends of silica particles were observed. In this manner, we wanted to improve Celecoxib solubility as well as its biocompatibility.

CHAPTER 4

4. EXPERIMENTAL

4.1 MATERIALS

Poly (ethylene glycol)-block-poly (propylene glycol)-block-poly (ethylene glycol) (Pluronic 123, $(C_3H_6O.C_2H_4O)_x$, M_w=5800 g/mole) and tetraethyl orthosilicate (TEOS, $(C_2H_5O)_4Si$ M_w=208.33 g/mole) were purchased from Aldrich. Aminopropyltriethoxysilane (APTES, $C_9H_{23}NO_3Si$) was purchased from Acros Organics. Celecoxib (Pfizer, Celebrex, 200 mg), 37% hydrochloric acid (HCl), NaOH, methanol, ethanol, hexane, boric acid (H_3BO_3) and ammonia were purchased from Sigma-Aldrich. KH_2PO_4 was purchased from Merck, and K_2HPO_4 was obtained from Riedel-Haen. All of the chemical reagents used are analytical grade. Deionized water was used during experiments. Protherm furnace having heat capacity up to 1300 ˚C, was used during all heating process.

4.2 SYNTHESIS OF SBA-15

SBA-15 particles were synthesized based on the technique written by Zhao et al. [36]. Nonionic triblock copolymer (Pluronic 123) (0.4 g) was dissolved in 46.5 ml 2.0 M HCl and 103.5 ml ethanol mixture at room temperature. When the mixture became colorless, the temperature was raised to 40 ˚C and 9.46 ml of the silica source TEOS was added to the mixture slowly with stirring. For 48 h, the mixture was aged at 90 ˚C and then filtered, washed and dried at ambient temperature. In the purpose of removing the surfactant template, calcination (160 ˚C, 1 h and then 550 ˚C, 12 h) was carried out [37].

Figure 8 represents the synthesis scheme of pure SBA-15 and Table 1 shows the precursors which were used during the experiments.
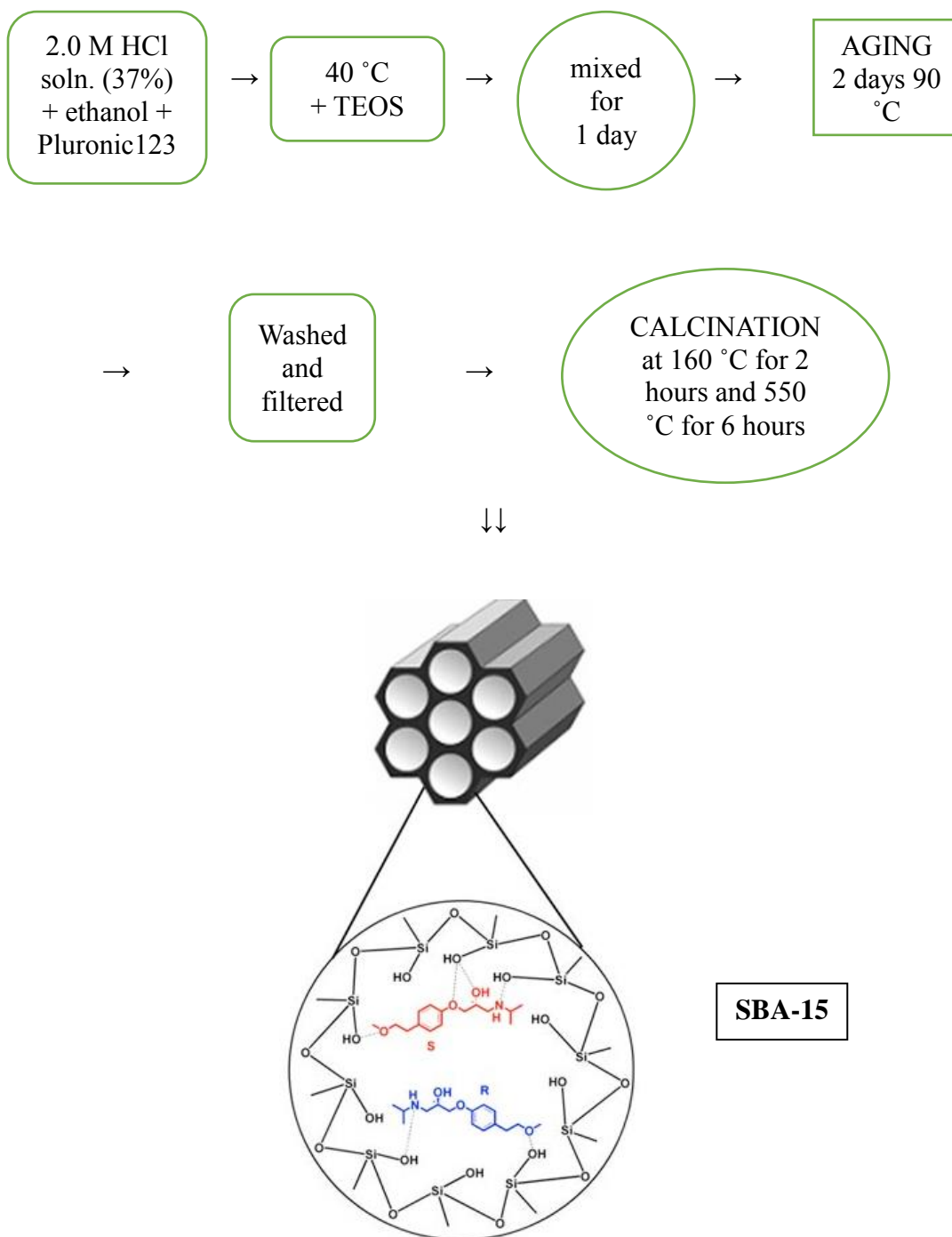
Figure 8 Schematic representation of synthesis of SBA-15.

Table 1 Precursors used for SBA-15 synthesis

Chemicals	m(g) or V(L)	Brand	d (g/mL)	MW (g/mol)
Pluronic 123	0.4 g	Aldrich	1.01	5800
TEOS	9.46 mL	Aldrich	0.93	208.3
Ethanol	103.5 mL	Sigma-Aldrich	0.79	46.07
HCl	46.5 mL	Sigma-Aldrich	1.20	36.46

4.3 SURFACE FUNCTIONALIZATION OF SBA-15

APTES (3- aminopropyltriethoxy silane)

$H_2N-(CH_2)_3-Si-(OCH_2CH_3)_3$
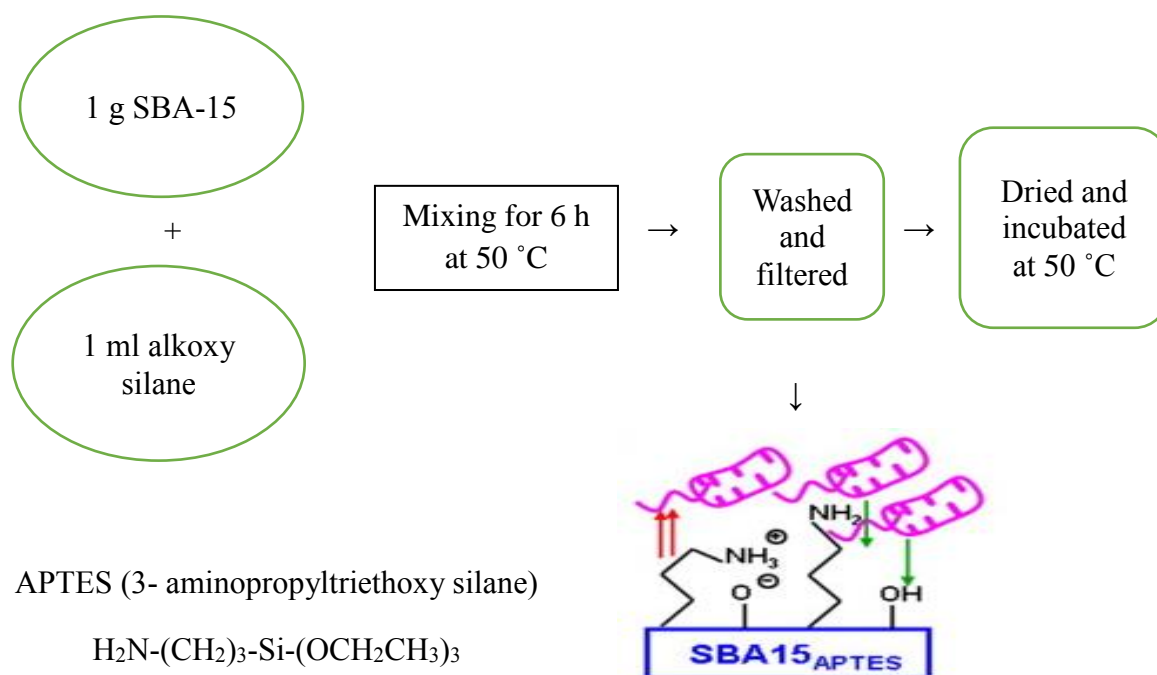
Figure 9 Schematic representation of synthesis of SBA-15-A.

Calcinated silica samples were functionalized by APTES with the post-grafting synthesis method. 1 g of SBA-15 and 1 ml APTES were stirred in 50 ml ethanol solution for 6 h at 50 ˚C, filtered and washed with deionized water. The samples were dried at room temperature for 1 day, the samples were incubated in an oven at 50 ˚C. Obtained white sample was named as SBA-15-A [37]. In Figure 9, amine functionalized SBA-

15 was seen and Table 2 shows the precursors which were used during the experiments.

Table 2 Precursors used for SBA-15-A synthesis

Chemicals	m(g) or V(L)	Brand	d (g/mL)	MW (g/mol)
APTES	9.46 mL	Acros Organics	0.93	208.3
Ethanol	50.0 mL	Sigma-Aldrich	0.79	46.07

4.4 SYNTHESIS OF BOROSILICATE
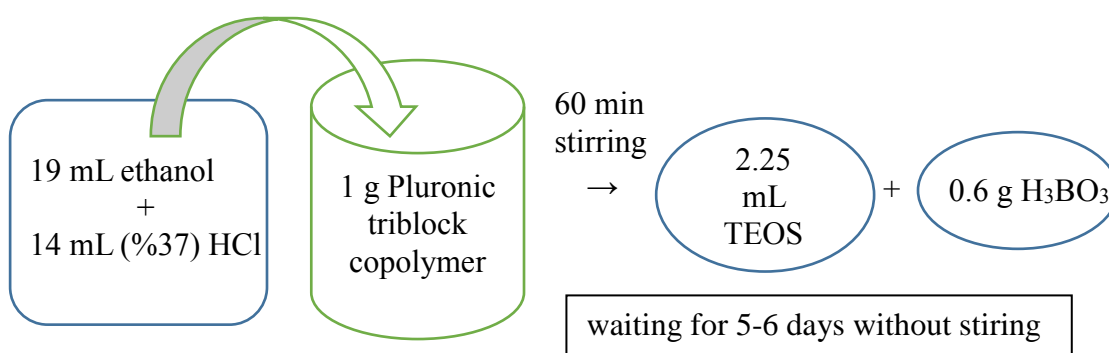
Figure 10 Schematic representation of synthesis of SBA-15-B.

Pluronic P123 triblock copolymer (1 g) was mixed with 19 ml ethanol and 14 ml 37% HCl under stirring within 90 minutes. TEOS (2.25 ml) was added to mixture slowly and obtained solution was stirred within 1 h. After adding 0.62 g H_3BO_3, the solution was mixed for a further 6 hours. Gel formation was seen after waiting for 6-7 days without stirring. During the calcination process of SBA-15-B, the gel was incubated in the oven at 160 ˚C for 2 h and 550 ˚C for 6 hours. The synthesis of boron doped SBA-15 was given in Figure 10 and Table 3 shows the precursors which were used during the experiments.

Table 3 Precursors used for SBA-15-B synthesis

Chemicals	m(g) or V(L)	Brand	d (g/mL)	MW (g/mol)
Pluronic 123	1 g	Aldrich	1.01	5800
TEOS	2.25 mL	Aldrich	0.93	208.3
Ethanol	19.0 mL	Sigma-Aldrich	0.79	46.07
HCl	14.0 mL	Sigma-Aldrich	1.20	36.46
H_3BO_3	0.62 g	Sigma-Aldrich	1.44	61.83

4.5 CELECOXIB LOADING

For Celecoxib loading, a liquid-phase grafting method was utilized. To determine the effect of solvents on drug loading; ethanol, methanol and hexane were chosen. SBA-15, SBA-15-A and SBA-15-B (0.1g for each) were separately taken and mixed with 0.1 g Celecoxib in 50 ml of ethanol, methanol or hexane within 48 hours at 25 ˚C under stirring. The nine samples obtained were denoted as SBA-15@Clx$_{eth}$, SBA-15@Clx$_{meth}$, SBA-15@Clx$_{hex}$, SBA-15-A@Clx$_{eth}$, SBA-15-A@Clx$_{meth}$, SBA-15-A@Clx$_{hex}$, SBA-15-B@Clx$_{eth}$, SBA-15-B@Clx$_{meth}$, and SBA-15-B@Clx$_{hex}$. The Celecoxib loaded silica samples were washed with their loading solvent and all of them were dried at room temperature. For quantitative determination of the drug, UV analyses were carried out at 254 nm wavelength. Beer-Lambert law was used to determine the drug concentration in silica samples. The mean value was calculated from 5 replicates. Drug loading efficiency could be calculated to the following equation:

$$\text{Drug Loading Efficiency} = \frac{\text{Weight of Celecoxib in sample}}{\text{Weight of carrier in sample}}$$

Table 4 Precursors used for Celecoxib loading to SBA-15, SBA-15-A and SBA-15-B

Chemicals	m(g) or V(L)	Brand	d (g/mL)	MW (g/mol)
SBA-15				60.08
SBA-15-A	0.1 g			
SBA-15-B				
Celecoxib	0.1 g	Pfizer		381.7
Methanol			0.79	32.04
Ethanol	50.0 mL	Merck	0.79	46.07
Hexane			0.65	86.18

4.6 CELECOXIB RELEASE

Celecoxib release from drug loaded silica particles was determined using UV spectro-photometry at 254 nm. Celecoxib loaded silica samples (0.5 g) were dissolved in 50 ml of a mixture of PBS, at 37 °C at pH=7.4 and pH=5.0. PBS was prepared with 13.97 g K_2HPO_4 and 2.69 g KH_2PO_4. The mixture of K_2HPO_4 and KH_2PO_4 were added to 1.0 L distilled water at room temperature and they were mixed. Drug release was determined at 30 minutes, 1 h, 2 h, 4 h, 6 h, 24 h, 72 h. Absorbance values taken from UV spectrophotometry were used for the calculation of the amount of Celecoxib released. Table 5 indicates used precursors during Celecoxib release from silica samples.

Table 5 Precursors used for Celecoxib release from SBA-15, SBA-15-A and SBA-15-B

Chemicals	m(g) or V(L)	Brand	d (g/mL)	MW (g/mol)
K_2HPO_4	13.97	Riedel-Haën	2.44	178.30
KH_2PO_4	2.69	Merck	2.34	136.02
H_2O	1.0 L	-	1.00	18.00

CHAPTER 5

5. CHARACTERIZATION

5.1 POWDER X-RAY DIFFRACTION (XRD)

Powder X-ray diffraction results were obtained with a Rigaku X-ray Diffractometer with a Miniflex goniometer operated at 30 kV and 15 mA Cu-Kα line (α=1.54 Å) as the source of X-ray. The scanning mode was chosen like continuous scanning.

5.2 SMALL ANGLE X-RAY SCATTERING (SAXS)

Small angle X-Ray scattering (SAXS) measurements were done with a Hecus X-Ray system (Graz, Austria SWAXS). A 2 kW X-Ray source was chosen and 0.04 and 0.550 Å range of a scattering pattern was utilized.

5.3 DIFFERENTIAL SCANNING ANALYSIS (DSC)

DSC (DSC N-650) analysis was carried out in the range between 25-200 ˚C at 5 ˚C/min heating rate.

5.4 THERMOGRAVIMETRIC ANALYSIS (TGA)

Thermogravimetric analysis was used in a Pyris 1 Perkin Elmer Thermogravimetric Analyzer with air condition in 30 and 600 ˚C temperature ranges and the heating rate of device is 10 ˚C/min.

5.5 UV-VIS SPECTROSCOPY

UV analysis method has been chosen for determination of samples quantitatively. In order to calculate concentration of species in solution, Beer Lambert law (A=ϵ.b.c) is used. UV-Vis results were obtained from a CARY 5000 UV-VIS-NIR Spectrophotometer for Celecoxib loading and release experiments.

5.6 FOURIER TRANSFORM INFRA RED SPECTROSCOPY (FT-IR)

FT-IR spectra for all mesoporous silica samples were measured with a Varian 1000 FT-IR (Scimitar FTS 1000) in 400-4000 cm^{-1} wavelength range in air with KBr pellets.

For preparation of KBr pellets, 20 mg sample and 180 mg KBr were taken and mixed homogenously. The mixture was placed in pelletizer and presses at 5000-10000 psi. Then transparent pellet was carefully taken and placed in the FT-IR sample holder for analysis. The chemical strutures of all silica samples were determined before and after Celecoxib loading by FT-IR.

5.7 NITROGEN - SORPTION

N_2 adsorption/desorption results have been conducted at 77 K in an Autosorb 6 (Quantachrome). Before measurement, every sample was degassed at 50 ˚C – 120 ˚C within 16 h. Pore characteristics were determined by using the BJH (Barret-Joyner-Halenda) and BET (Brunauer-Emmett-Teller) methods.

5.8 SCANNING ELECTRON MICROSCOPE (SEM)

SEM images were taken with Zeiss SUPRA 50 VP at 80 kV. In order to improve imaging quality, the samples were coated with a thin layer of conducting material, Au/Pd alloy.

5.9 TRANSMISSION ELECTRON MICROSCOPY (TEM)

TEM images were taken with JEOL JEM 2100F STEM and a JEOL JEM 2100F Field Emission Gun at 120 kV. Before the analyses, samples were washed in ethanol in the Elma S 30 H ultrasonic bath for 15 minutes.

CHAPTER 6

6. RESULTS & DISCUSSION

SBA-15, amine functionalized SBA-15 (SBA-15-A) and boron doped SBA-15 (SBA-15-B) were synthesized, their Celecoxib loading and release amounts were investigated. For characterization of these samples, using x-ray diffraction (XRD), N_2 adsorption - desorption, small – angle x-ray spectrometry (SAXS), Fourier transform infra-red spectroscopy (FT-IR), differential scanning calorimetry (DSC), scanning electron microscope (SEM), ultraviolet-visible spectrometry (UV-vis), transmission electron microscope (TEM) and thermogravimetric analysis (TGA) were used.

6.1 POWDER X-RAY DIFFACTION PATTERN OF SBA-15 PARTICLES

For characterization of SBA-15, SBA-15-A, SBA-15-B and Celecoxib loaded forms of that samples, XRD analysis was used. Celecoxib has triclinic unit cell with dimensions of a=10.136 Å, b=16.778 Å, c=5.066 Å crystal lattice parameters and α=97.62˚, β=100.65˚, ɣ=95.95˚ with the most intense peaks at 2θ=18.8˚ and 2θ=25.1˚ [45].

Figure 11, 12, 13 show the XRD pattern of pure, amine functionalized, boron doped silica samples and Celecoxib loaded silica samples in ethanol, methanol and hexane solvents. According to a research paper published by Popovici, SBA-15 mesoporous silica has two intense peaks in 2θ degree between 0.9-1.05 and 1.8-2.0 [46]. In Figure 11, crystalline peaks were seen for SBA-15@Clx$_{eth}$ and SBA-15@Clx$_{hex}$. In the Figure 11, after incorporation of Celecoxib into the mesopores of SBA-15 in methanol, no characteristic diffraction peaks related to crystalline form were observed, which presented that Celecoxib stayed in amorphous state in this sample. On the other hand, crystallization of Celecoxib was reported to be hindered when Celecoxib settled into SBA-15 mesopores [47]. SBA-15@Clx$_{eth}$ also showed few characteristic peaks of Celecoxib, indicating that reduction of crystallinity. The intensity of SBA-15 was reduced, characteristic peaks of Celecoxib were started to be observed clearly. However,

SBA-15@Clx_hex clearly indicated all diffraction peaks of Celecoxib showing the persistence of crystalline Celecoxib in the SBA-15@Clx_hex material. Because the intensity of amorphous SBA-15 line is decreased, all the peaks of Celecoxib are seen apparently.
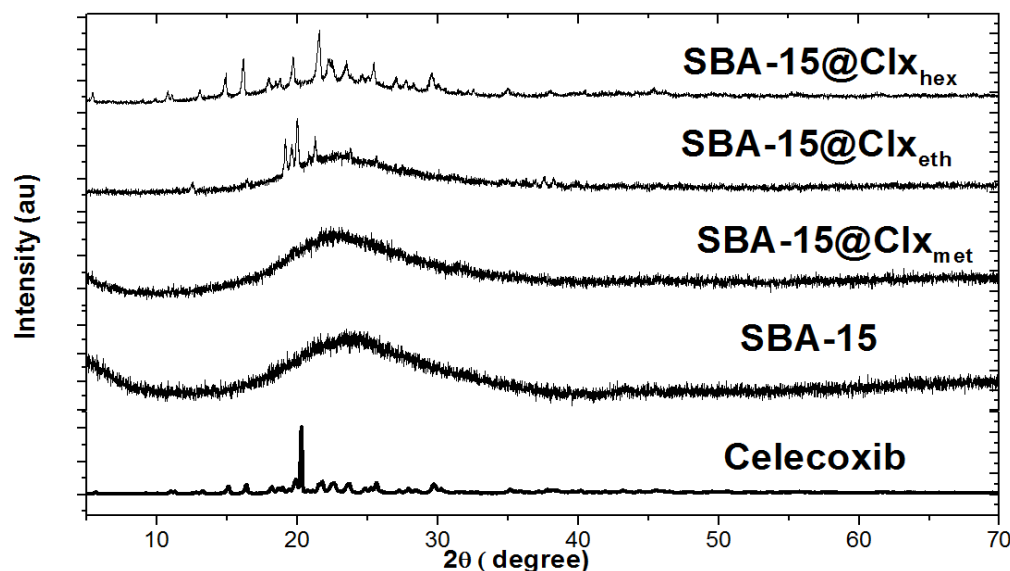
Figure 11 Wide angle powder XRD pattern of SBA-15, SBA-15@Clx_eth, SBA-15@Clx_meth, SBA-15@Clx_hex and Celecoxib.

In Figure 12, for drug loaded SBA-15-A and SBA-15-B samples in different solvents, the same behavior was observed in the diffraction patterns. Again SBA-15-A and SBA-15-A@Clx_meth indicated their amorphous phases, crystalline peaks were appeared in other silica samples. As seen in Figure 13, 2θ peaks are in the range of $14°$ and $28°$, which belong to boron oxide (B_2O_3). After the functionalization of SBA-15 with amino propyl groups or boron doped SBA-15 and loading with Celecoxib, peak intensities were reduced but peaks became broader. The varieties in the diffraction patterns of Celecoxib loaded samples can be related to the arrangement of molecules in the crystal forms with solvent effect [48].
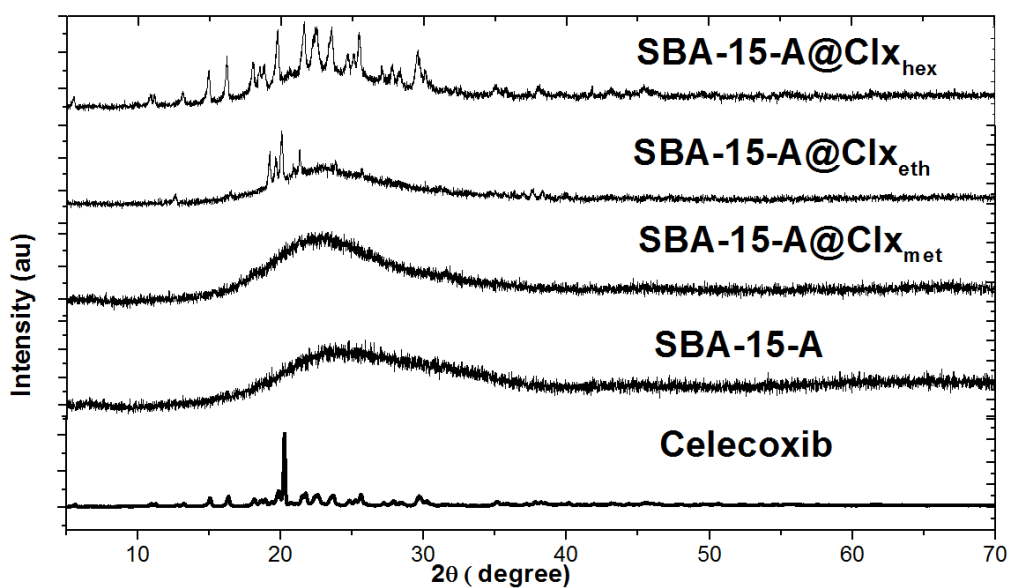
Figure 12 Wide angle powder XRD pattern of SBA-15-A, SBA-15-A@Clx$_{eth}$, SBA-15-A@Clx$_{meth}$, SBA-15-A@Clx$_{hex}$ and Celecoxib.
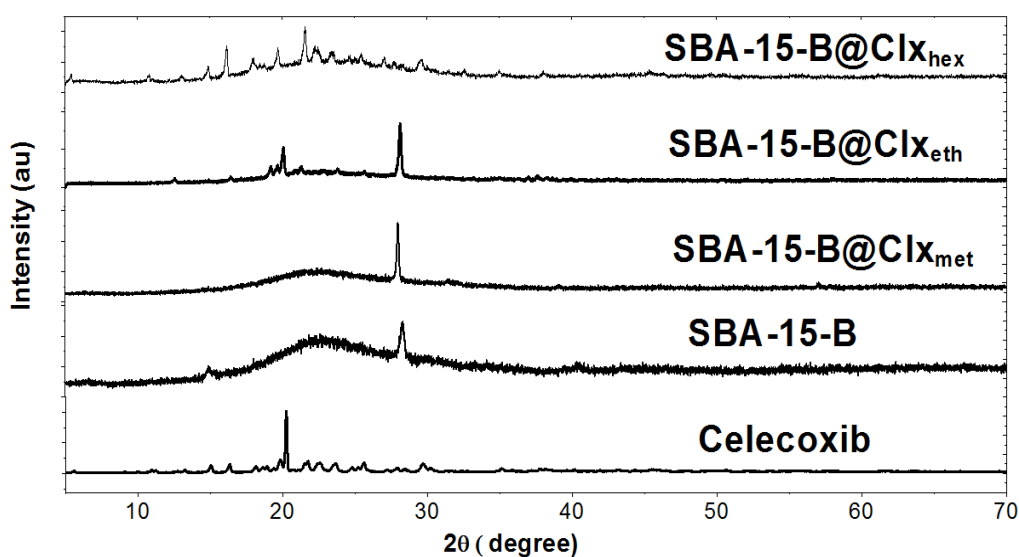
Figure 13 Wide angle powder XRD pattern of SBA-15-B, SBA-15-B@Clx$_{eth}$, SBA-15-B@Clx$_{meth}$, SBA-15-B@Clx$_{hex}$ and Celecoxib.

6.2 SMALL ANGLE X-RAY SCATTERING (SAXS)

Small angle diffraction patterns for SBA-15 and modified SBA-15 samples are illustrated in Figure 14. The diffractograms of SBA-15-A and SBA-15-B displayed nearly the same diffraction pattern with SBA-15. The – d spacing values were calculated by

25

using Bragg Law ($\lambda=2d.\sin\theta$ and $q=4\pi.\sin\theta/\lambda$). The highest intensity peak of diffraction patterns were indexed as (100) and very small intensities of (110) and (200) peaks were available only in SBA-15 and its drug loaded with methanol form. These peaks indicating P6mm hexagonal pore structure characteristic and having well-ordered mesoporous structures which were reported in an article written by Glatter, Khodakov and Kang et al [49, 50, 51]. However small intensity peaks of pattern were not observed in amine functionalized and boron added form of SBA-15 even SBA-15 drug loaded in ethanol and hexane form. Moreover, borosilicate samples had broader peaks than SBA-15 samples that shows decreased order of pores. The characteristic Bragg diffraction peaks of each material stay constant after drug loading process showing that the mesoporous structure of silica materials are preserved.

a   **b**   **c**
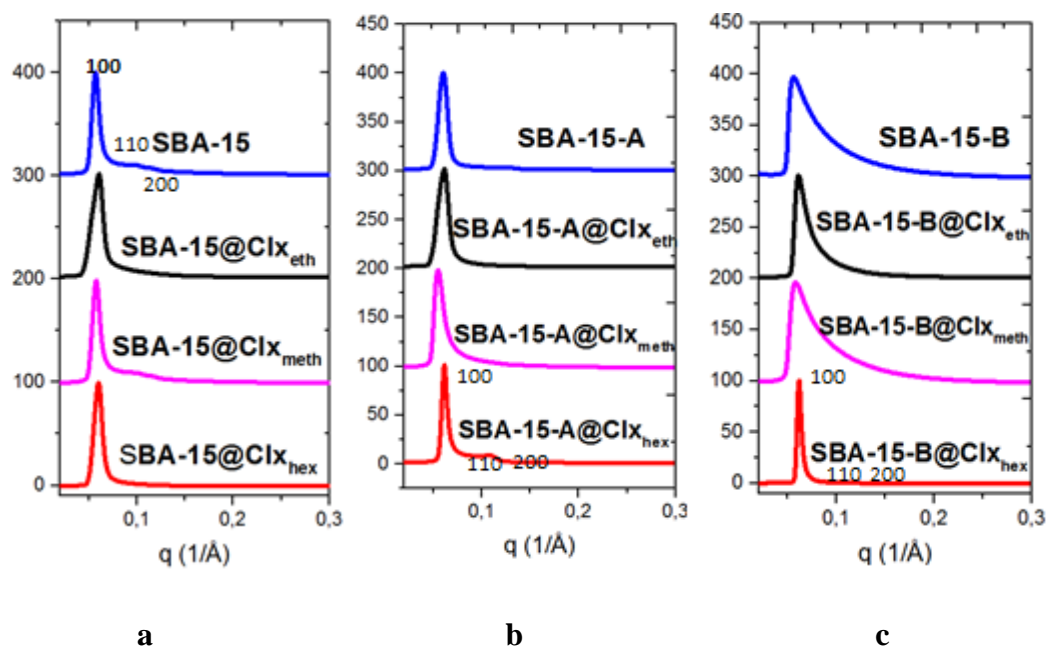
Figure 14 Small angle powder XRD patterns of a) SBA-15, SBA-15@Clx$_{eth}$, SBA-15@Clx$_{meth}$, SBA-15@Clx$_{hex}$; b) SBA-15-A, SBA-15-A@Clx$_{eth}$, SBA-15-A@Clx$_{meth}$, SBA-15-A@Clx$_{hex}$; c) SBA-15-B, SBA-15-B@Clx$_{eth}$, SBA-15-B@Clx$_{meth}$, SBA-15-B@Clx$_{hex}$.

6.3 FTIR ANALYSIS

SBA-15 samples, SBA-15 samples loaded with Celecoxib mixed in three solvents were analyzed in FTIR in order to examine the infrared spectra. FTIR spectrum of Celecoxib and its indicated chemical grups are seen in Figure 15.
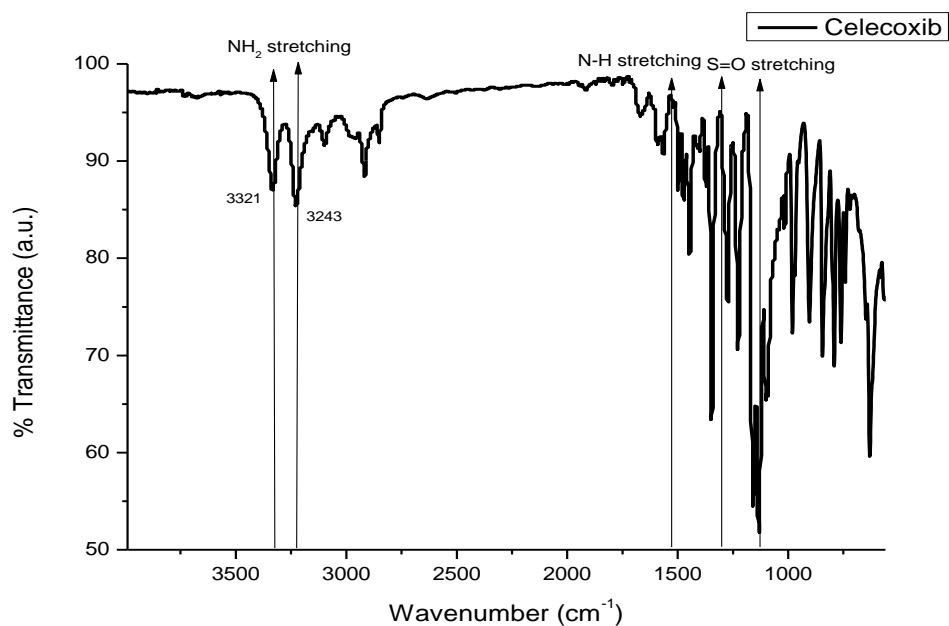
Figure 15 The chemical groups of Celecoxib in FT-IR spectra.

The FT-IR spectra model of SBA-15 and its Celecoxib loaded forms in ethanol, methanol, and hexane are shown in Figure 16. All samples showed a broad band at near 1100 cm^{-1} which is related to Si-O-Si asymmetric stretching vibration mode [52]. Symmetric vibration modes and bending vibrations of condensed silica network appeared at 800 cm^{-1} and 500 cm^{-1}, respectively. Surface silanol groups in the stretching vibrational mode appeared in the 3740-3000 and around 900 cm^{-1} range. In the presence of Celecoxib, a double sharp peak at 3342-3235 cm^{-1} and two single peaks at 1348 and 1164 cm^{-1} were observed with SBA-15@Clx$_{hex}$ [52]. Moreover, C-H stretching arising from ethoxy groups were in the range of 2939-2908 cm^{-1} of CH stretching and 1470 cm^{-1} of hydrocarbon chain [52, 54].
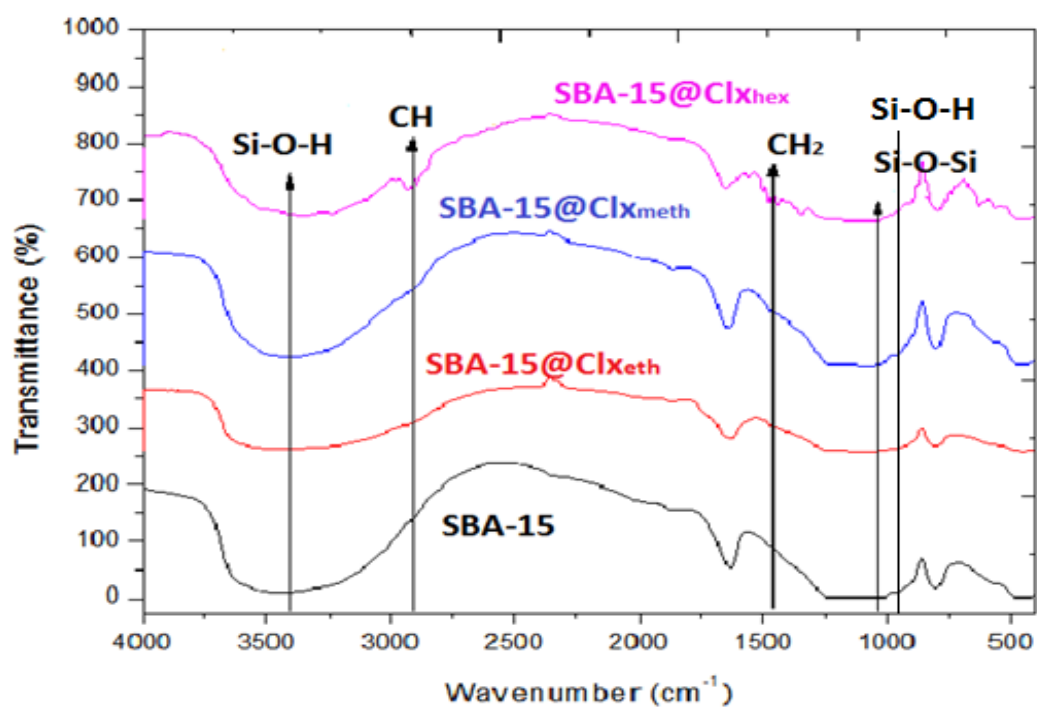
Figure 16 FT-IR spectra of **SBA-15, SBA-15@Clx$_{eth}$, SBA-15@Clx$_{meth}$, and SBA-15@Clx$_{hex}$.**
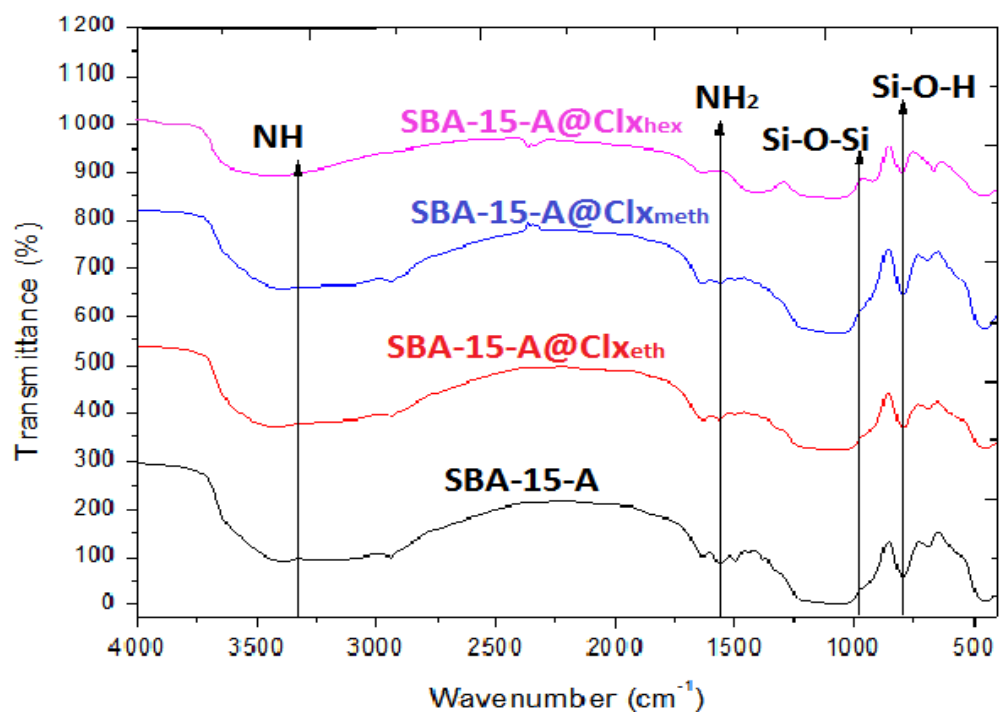
Figure 17 FT-IR spectra of SBA-15-A, SBA-15-A@Clx$_{eth}$, SBA-15-A@Clx$_{meth}$, and SBA-15-A@Clx$_{hex}$.

Asymmetric NH stretching bands were appeared in the SBA-15-A samples that were surface functionalized with aminopropyl groups (Figure 17). N-H stretching bands were seen at 3380-3310 cm^{-1} with an asymmetric NH_2 bending at 1600 cm^{-1}. After functionalization of SBA-15, SiO_2 stretching bands changed to 1085 cm^{-1}, 804 cm^{-1} and 456 cm^{-1} [44]. The peaks at 3342-3235 cm^{-1} and 1348-1164 cm^{-1} in the SBA-15-A@Clx$_{hex}$ indicate that Celecoxib still existed in a crystal form.
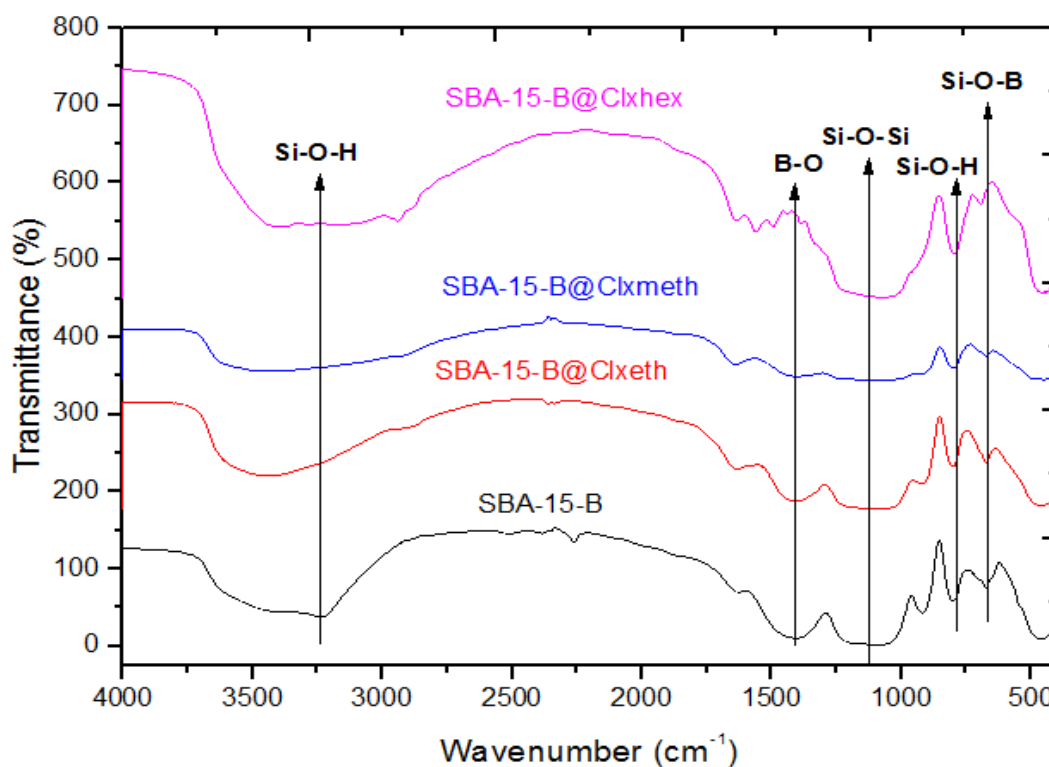
Figure 18 FT-IR spectra of SBA-15-B, SBA-15-B@Clx$_{eth}$, SBA-15-B@Clx$_{meth}$, and SBA-15-B@Clx$_{hex}$.

In Figure 18, chemical groups of boron doped silica samples are seen. In this figure, Si-O-H bond spectral data can be clearly identified at 780 and 3420-3474 cm^{-1}; the strong bands at 1082 cm^{-1}, 800 cm^{-1} and 462 cm^{-1} can be attributed to the Si-O-Si bond. The Si-O-B bond linkage was seen at 668 cm^{-1} and B-O stretching vibrations were observed at 1400-1500 cm^{-1}. The addition of boron caused small peaks at 570 cm^{-1} and 1190 cm^{-1} [48]. FT-IR peaks of Celecoxib again were seen only in SBA-15-B@Clx$_{hex}$.

29

6.4 N_2 – ADSORPTION – DESORPTION ANALYSIS

According to the IUPAC classification, all samples analyzed presented typical irreversible type IV isotherms, which confirm their mesoporous structure. [44].

Table 6 summarizes the textural properties of silica samples. Pure SBA-15 had the highest specific surface area of 564 $m^2 g^{-1}$, pore volume of 0.847 $cm^3 g^{-1}$ and pore diameter of 7.82 nm. After functionalization of SBA-15, its pore volume was reduced due to the addition of functional organic groups on the surface. SBA-15@Clx$_{eth}$ and SBA-15@Clx$_{meth}$ had relatively larger surface areas unlike SBA-15@Clx$_{hex}$, which had a very small surface area.

Table 6 Specific surface area, pore volume and pore diameter of SBA-15 samples before and after Celecoxib loading in ethanol, methanol and hexane

Sample	Specific Surface Area (S_{BET}) ($m^2 g^{-1}$)	Pore Volume (V_p) ($cm^3 g^{-1}$)	Pore Diameter (nm)
SBA-15	**564**	**0.847**	**7.82**
SBA-15@Clx$_{eth}$	473	0.514	5.72
SBA-15@Clx$_{meth}$	468	0.689	9.72
SBA-15@Clx$_{hex}$	9.36	0.036	3.92
SBA-15-A	**235**	**0.398**	**5.63**
SBA-15-A@Clx$_{eth}$	44.9	0.065	4.36
SBA-15-A@Clx$_{meth}$	27.2	0.053	4.41
SBA-15-A@Clx$_{hex}$	20.2	0.059	1.98
SBA-15-B	473	0.445	2.46
SBA-15-B@Clx$_{eth}$	**154**	**0.373**	**1.44**
SBA-15-B@Clx$_{meth}$	117	0.198	1.48
SBA-15-B@Clx$_{hex}$	10.8	0.0193	1.47

The pore volume showed similar trends in SBA-15 and SBA-15-B, while Celecoxib loaded SBA-15 and SBA-15-B samples in hexane showed the smallest pore volume, so it could be concluded that high amount of drug loaded into pores in hexane solvent. However, increase in pore volume may lead to Celecoxib attachment on outer surface of samples.

6.4.1 BRUNAUER-EMMETT-TELLER METHOD (BET)

BET (Brunauer-Emmett-Teller) method was used for analyzing surface properties and pore characteristics in silica samples. At constant temperature and changing pressure, gas adsorption volume and desorption on the silica surface are determined. By using BET method resulting in this measurement; surface area, pore diameter and pore volume of silica samples are investigated.

The N_2 isotherms of SBA-15 samples in different solvents are shown in Figure 19. A uniform pore size of SBA-15 was manifested by the noticeably sharp increase at $P/P_0=0.8$ [53]. In addition, the steep curve is influenced by capillary condensation in cylindrical pores [55]. The shape of the isotherm curves for drug loaded SBA-15 samples showed variations with different solvents that indicate a decrease in uniformity. SBA-15@Clx$_{meth}$ and SBA-15@Clx$_{eth}$ showed similar peak behaviors; nevertheless, SBA-15@Clx$_{meth}$ had a more uniform pore size distribution. SBA-15@Clx$_{hex}$ showed a small peak at around 0.9 that related to a narrow pore size distribution and decrease in the order of the mesostructured property of silica samples.
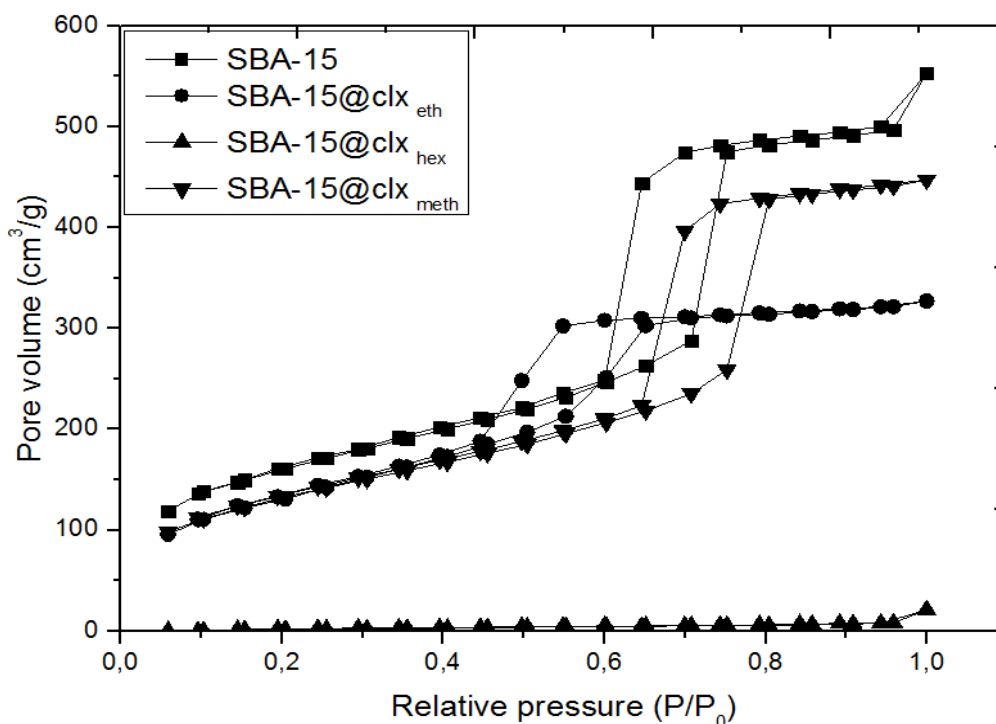
Figure 19 BET isotherms of SBA-15, SBA-15@Clx_eth, SBA-15@Clx_meth, and SBA-15@Clx_hex.

Figure 20 and Figure 21 show the BET isotherms of empty SBA-15-A, SBA-15-B samples and Celecoxib loaded SBA-15-A and SBA-15-B samples in three different solvents, respectively. Amine functionalized and Celecoxib loaded silica samples shift down with the capillary condensation step to lower pressures. Capillary condensation takes place in the P/P_0=0.40-0.55 and adsorption shift confirms that pore filling as well as decreased pore size value [55]. SBA-15 and SBA-15-A samples exhibit higher surface area and pore width than the borosilicate materials. Decreased BET surface area and the pore diameter in SBA-15-B samples with higher boron content maybe diminish the order of mesostructure [56].
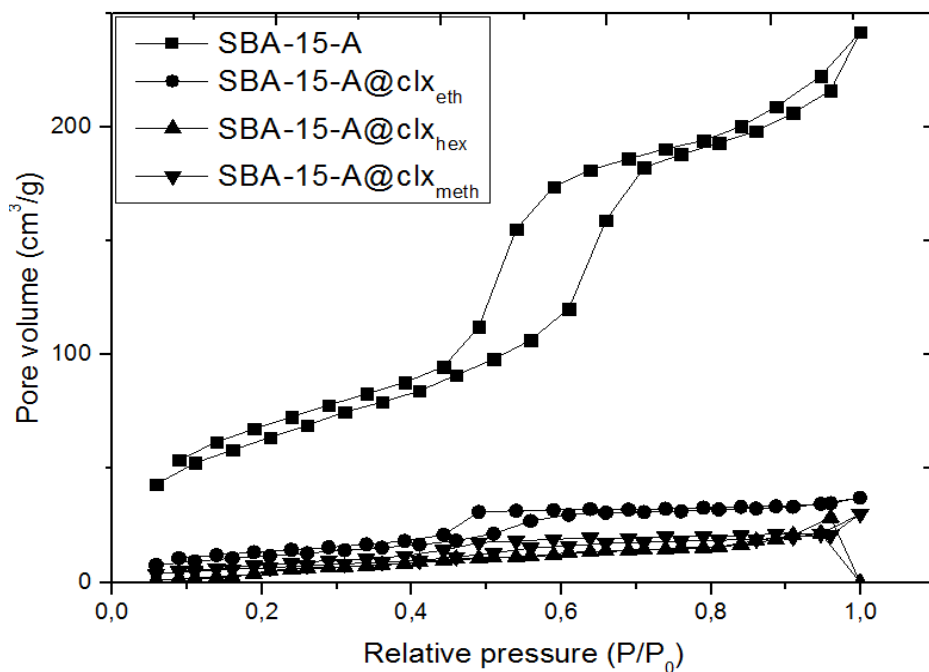
Figure 20 BET isotherms of SBA-15-A, SBA-15-A@Clx$_{eth}$, SBA-15-A@Clx$_{meth}$, and SBA-15-A@Clx$_{hex}$.
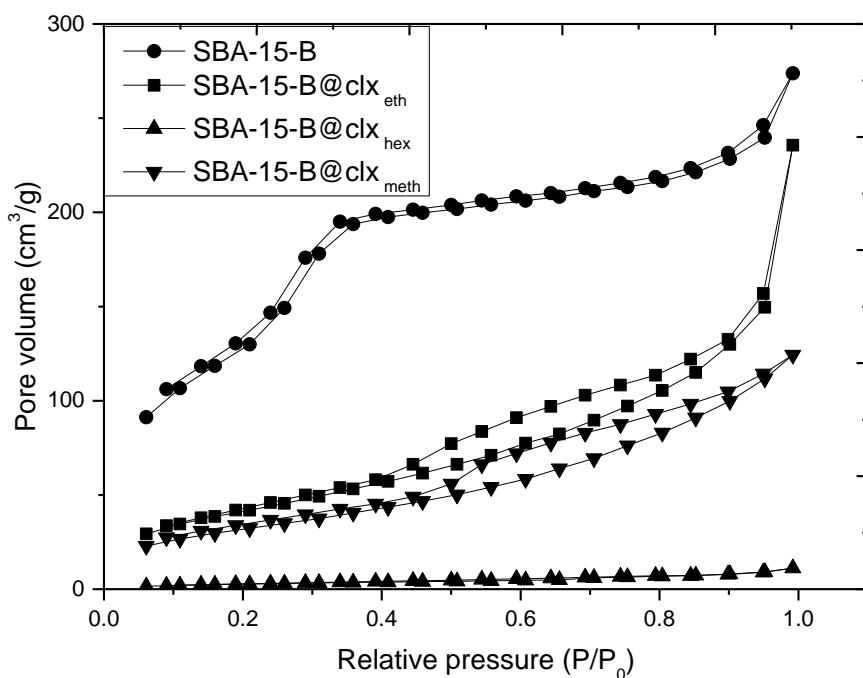
Figure 21 BET isotherms of SBA-15-B, SBA-15-B@Clx$_{eth}$, SBA-15-B@Clx$_{meth}$, and SBA-15-B@Clx$_{hex}$.

6.4.2 BARRET JOYNER HALENDA ANALYSIS (BJH)

BJH adsorption was determined for the pore size distribution of samples. All samples showed a typical irreversible type IV nitrogen adsorption isotherm with an H1 hysteresis loop.

The pore size distributions of SBA-15, SBA-15-A, SBA-15-B and Celecoxib loaded forms in different solvents are observed in Fig. 22, 23 and 24, respectively. Pure SBA-15 samples have 5.0-7.5 nm range pore size distribution. Pure SBA-15-A have a pore size distribution in the range of 3.5-5.5 nm. After Celecoxib loading to silica samples, narrower pore size distribution are obtained. SBA-15-B samples have less ordered mesopores, and Celecoxib loaded SBA-15-B samples have lowest pore sizes.
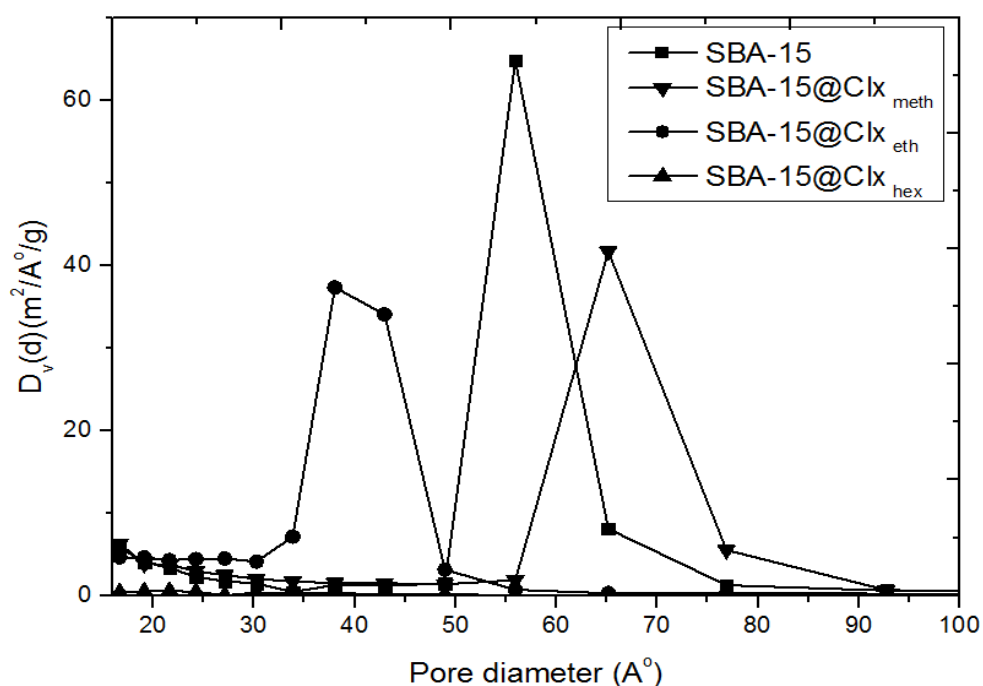
Figure 22 Pore size distribution of SBA-15, SBA-15@Clx$_{eth}$, SBA-15@Clx$_{meth}$, and SBA-15@Clx$_{hex}$.
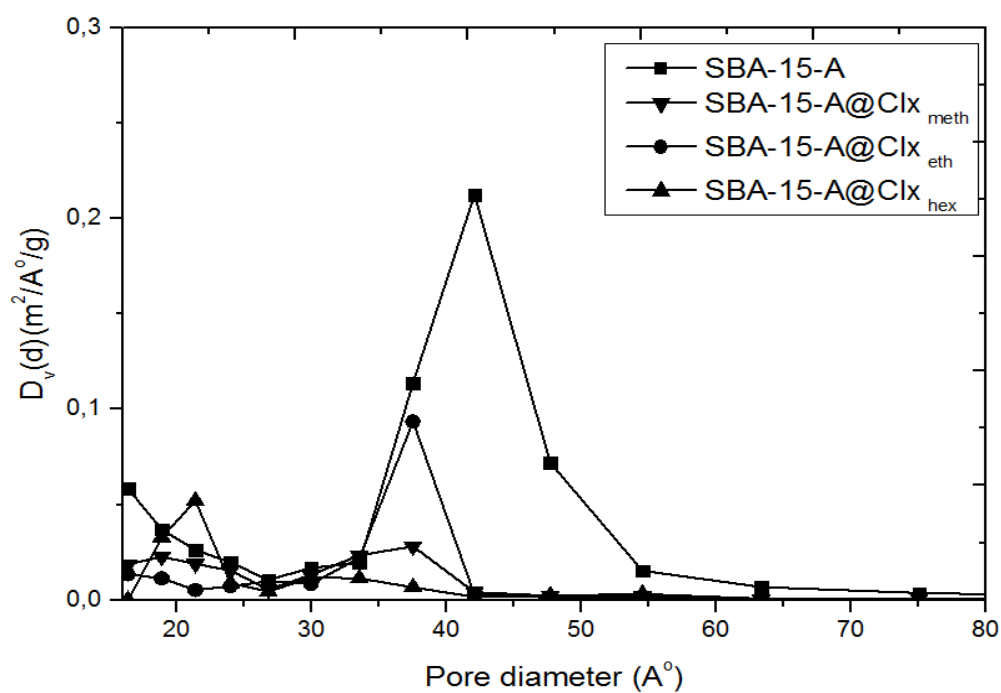
Figure 23 Pore size distribution of SBA-15-A, SBA-15-A@Clx$_{eth}$, SBA-15-A@Clx$_{meth}$, and SBA-15-A@Clx$_{hex}$.
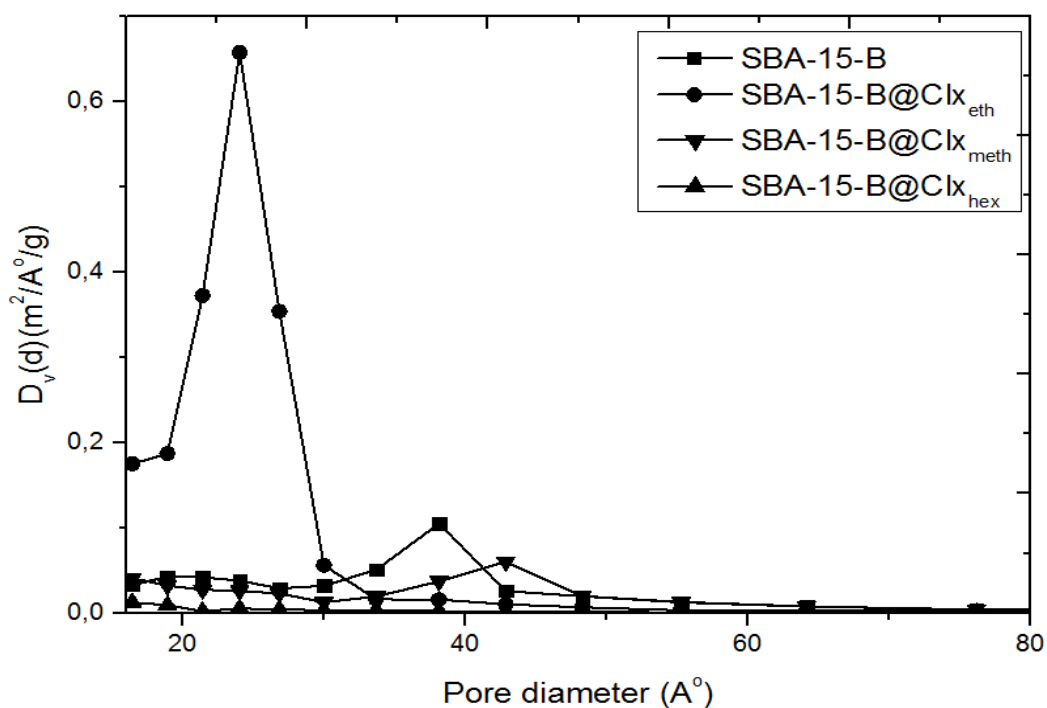
Figure 24 Pore size distribution of SBA-15-B, SBA-15-B@Clx$_{eth}$, SBA-15-B@Clx$_{meth}$, and SBA-15-B@Clx$_{hex}$.

6.5 DIFFERENTIAL SCANNING CALORIMETRY (DSC) ANALYSIS

To determine the physical state of Celecoxib loaded silica samples, DSC analysis was carried out (Figure 25, 26, 27). For Celecoxib, a single sharp endothermic melting point was observed between 161-165 ˚C [45].

In Figure 25, 26 and 27, DSC analysis results of silica samples were seen clearly. None of the silica samples prepared in methanol or ethanol showed endothermic peaks because of their amorphous state. However, Celecoxib loaded silica samples in hexane showed an endothermic peak, which confirmed that the drug was in crystalline form when loaded in mesoporous silica.
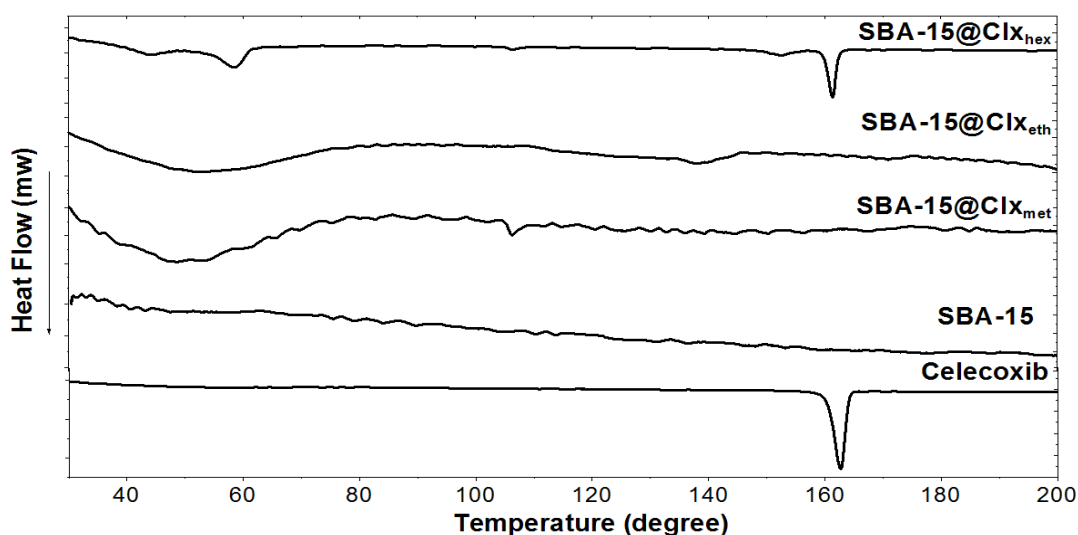
Figure 25 DSC thermograms of SBA-15, SBA-15@Clx$_{eth}$, SBA-15@Clx$_{meth}$, and SBA-15@Clx$_{hex}$.
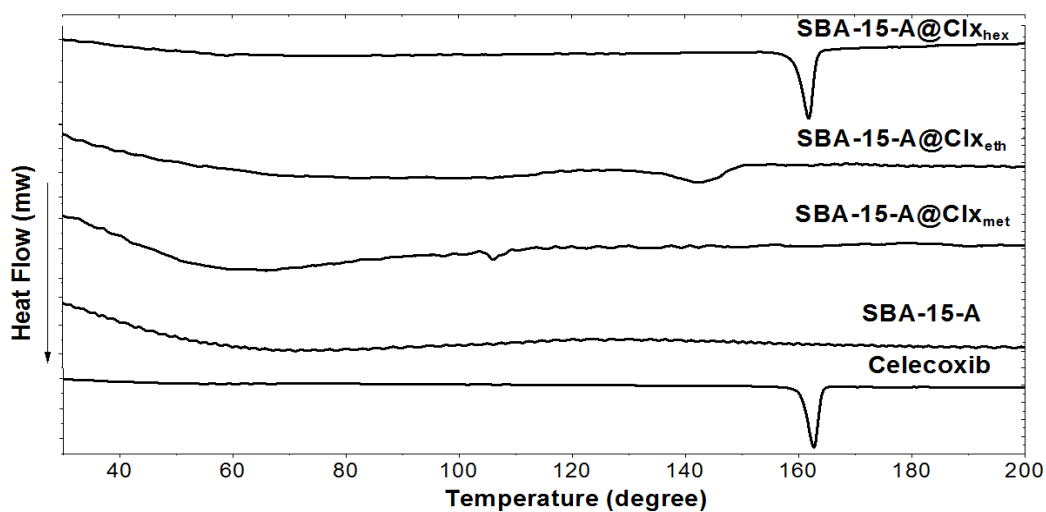
Figure 26 DSC thermograms of SBA-15-A, SBA-15-A@Clx$_{eth}$, SBA-15-A@Clx$_{meth}$, and SBA-15-A@Clx$_{hex}$.
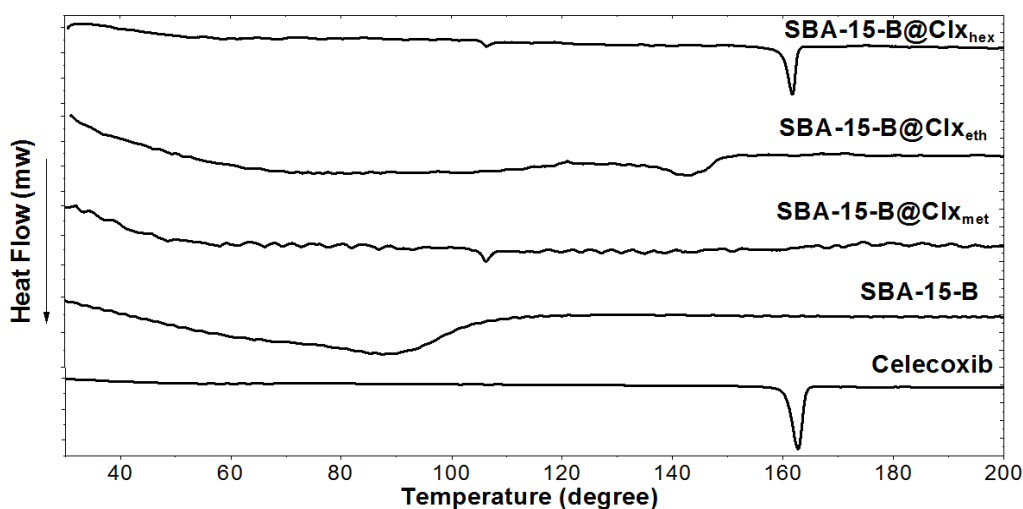
Figure 27 DSC thermograms of SBA-15-B, SBA-15-B@Clx$_{eth}$, SBA-15-B@Clx$_{meth}$, and SBA-15-B@Clx$_{hex}$.

6.6 THERMOGRAVIMETRIC ANALYSIS (TGA)

Thermogravimetric analysis (TGA) determined the organic groups in the silica samples [58]. As shown in Figure 28, 29, and 30; the weight loss peaks in silica samples were seen in the temperatures between 200-600 °C, which indicated thermal degradation of Celecoxib. Weight loss, observed up to a temperature of 200 °C, was likely to have resulted from a loss of adsorbed water and gases like CO_2, NH_3, NO_x, SO_y. As

37

seen in Figure 29, at temperatures above 200 ˚C, mass loss occurred because of the aminopropyl groups in SBA-15-A [44].

Maximum weight loss was observed in Celecoxib loaded silica samples in hexane which also indicates that these samples had the highest amount of drug loading. Minimum weight losses were observed for all Celecoxib loaded in methanol solvent. All of these results will support to UV drug loading values.
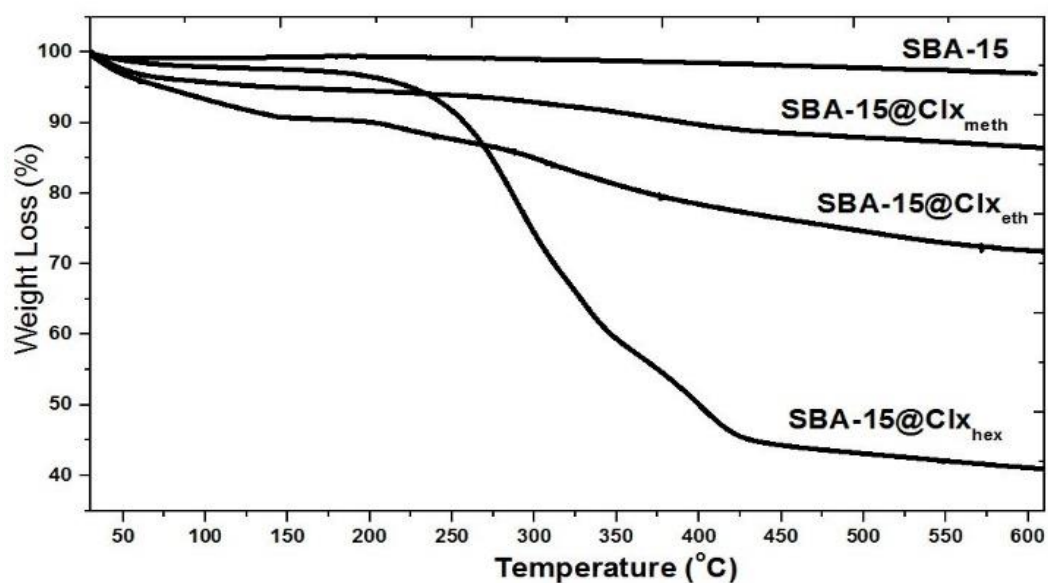
Figure 28 % Weight loss of SBA-15, SBA-15@Clx$_{eth}$, SBA-15@Clx$_{meth}$, and SBA-15@Clx$_{hex}$.
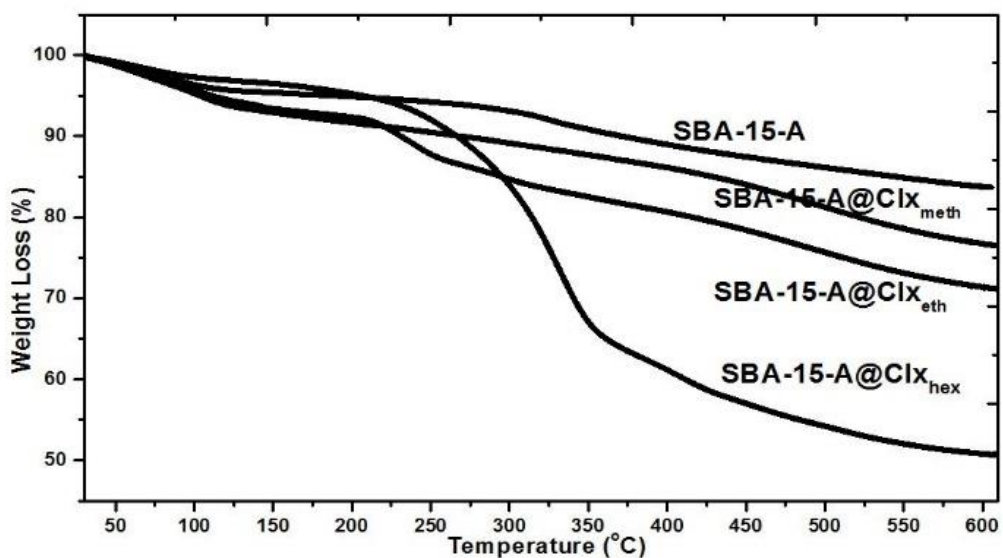
Figure 29 % Weight loss of SBA-15-A, SBA-15-A@Clx_eth, SBA-15-A@Clx_meth, and SBA-15-A@Clx_hex.
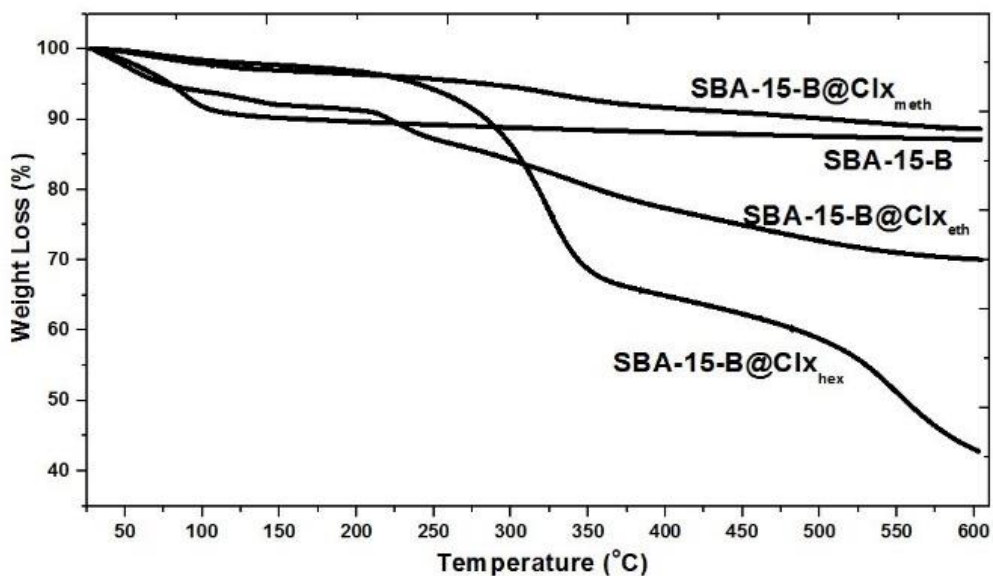
Figure 30 % Weight loss of SBA-15-B, SBA-15-B@Clx_eth, SBA-15-B@Clx_meth, and SBA-15-B@Clx_hex.

6.7 TRANSMISSION ELECTRON MICROSCOPY (TEM) ANALYSIS

Transmission electron microscopy (TEM) images of silica samples are illustrated in Figures 31, 32, and 33. SBA-15 and SBA-15-A were observed to have well-ordered

hexagonal structures, however TEM images of SBA-15-B samples have not well-ordered structures enough.

According to TEM images, after Celecoxib loading, SBA-15@Clx$_{eth}$, SBA-15@Clx$_{meth}$, SBA-15@Clx$_{hex}$ maintained their ordered and stable structures. They all had hexagonal and uniform structures. SBA-15-A and SBA-15-A@Clx$_{eth}$ had nearly the same ordered channels of arrays and they still possessed hexagonal mesochannels in the domain. It may be concluded from TEM images of SBA-15-A@Clx$_{eth}$, the drug particles were accumulated on the surface and inside the mesochannels of SBA-15-A [59].

In SBA-15-A@Clx$_{meth}$, disordering of silica samples started. Moreover, SBA-15-A@Clx$_{hex}$ did not show a hexagonal mesostructure, so it was concluded that hexane, as a nonpolar solvent, may change the morphology of the silica particles. SBA-15-B showed a less ordered mesoporous structure because of increased boron content; boron has been shown to decrease the ordered structure of silica [57]. In addition TEM images of SBA-15-B@Clx$_{eth}$ show more ordered structure according to solvent used in loading process. In addition, hexane may also have contributed to the altered morphology of SBA-15-B@Clx$_{hex}$.
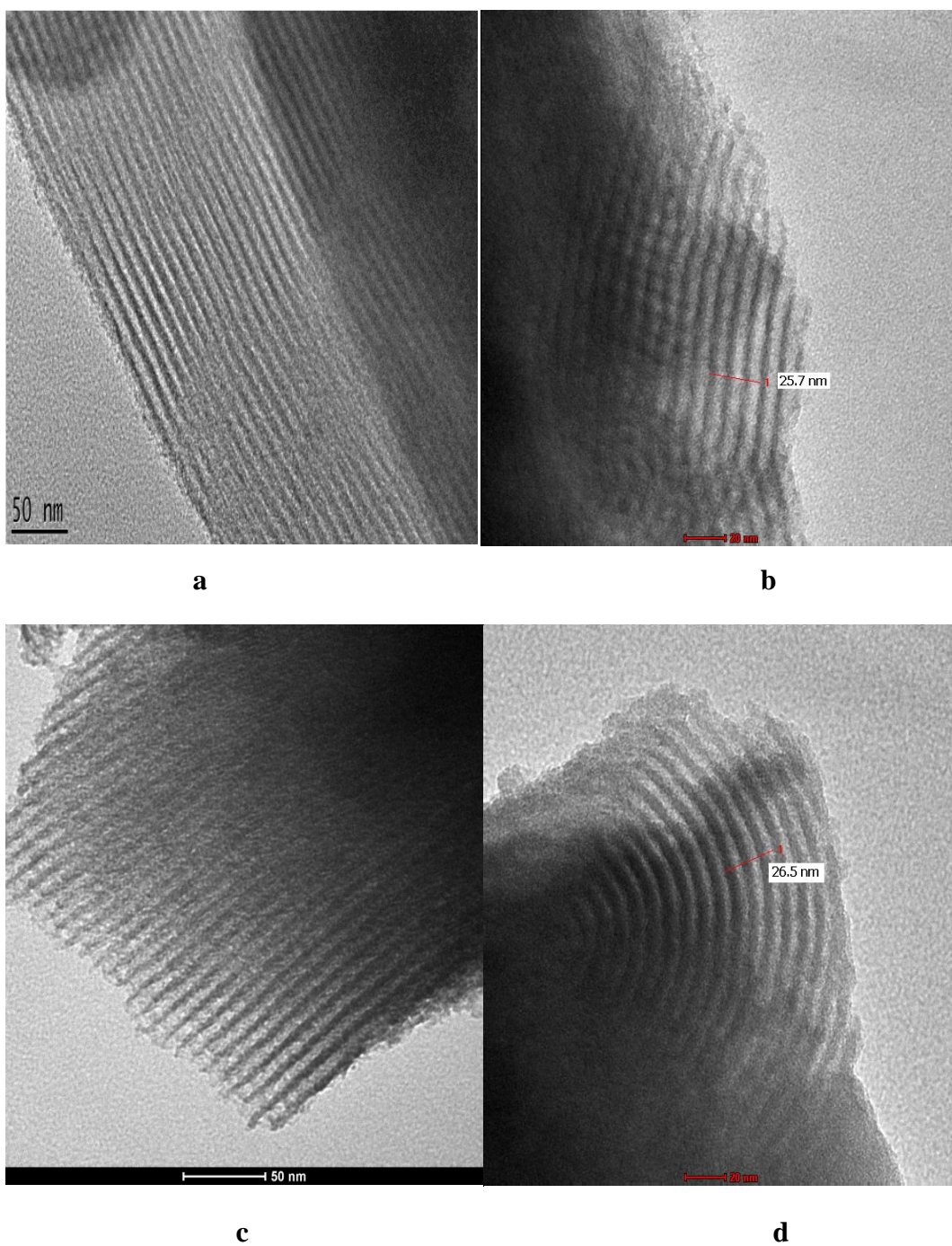
Figure 31 TEM images of a) SBA-15 (50 nm), b) SBA-15@Clx$_{eth}$, (20 nm), c) SBA-15@Clx$_{meth}$ (50 nm), d) SBA-15@Clx$_{hex}$ (20 nm).
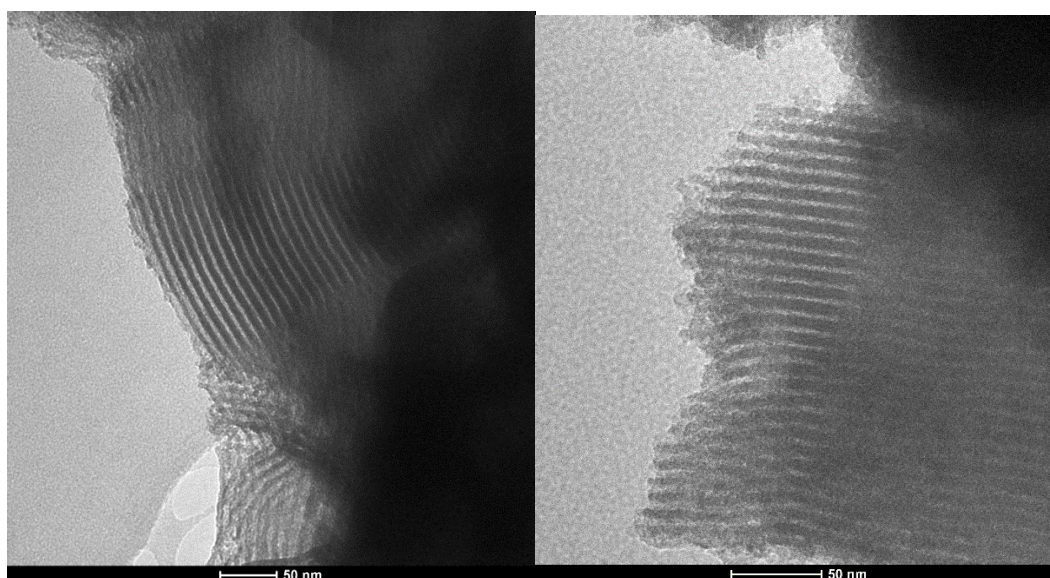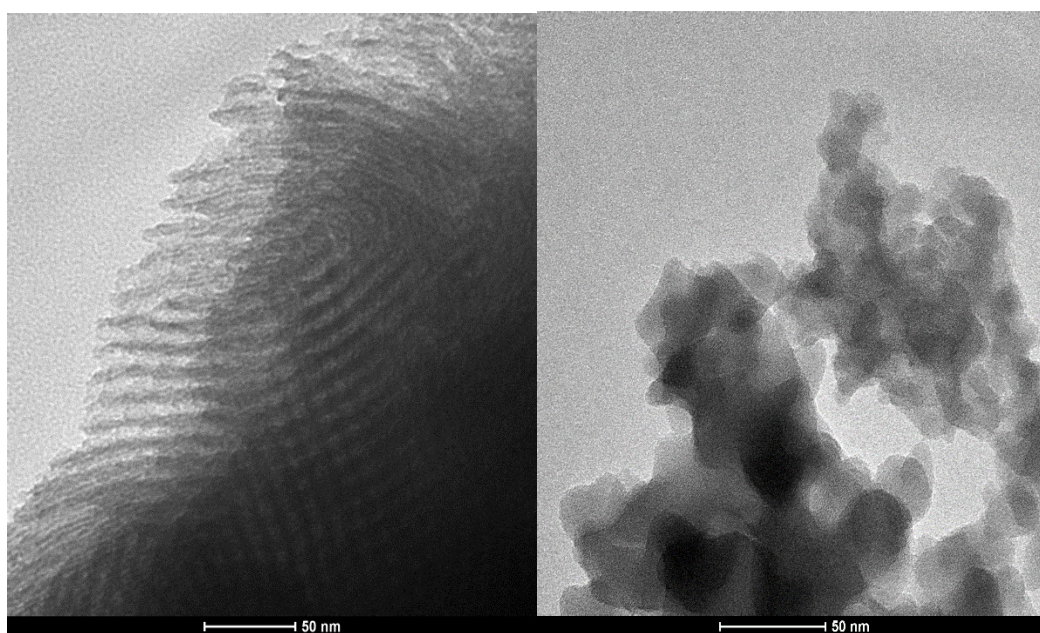
Figure 32 TEM images of a) SBA-15-A (50 nm), b) SBA-15-A@Clx$_{eth}$ (50 nm), c) SBA-15-A@Clx$_{meth}$ (50 nm), d) SBA-15-A@Clx$_{hex}$ (50 nm).
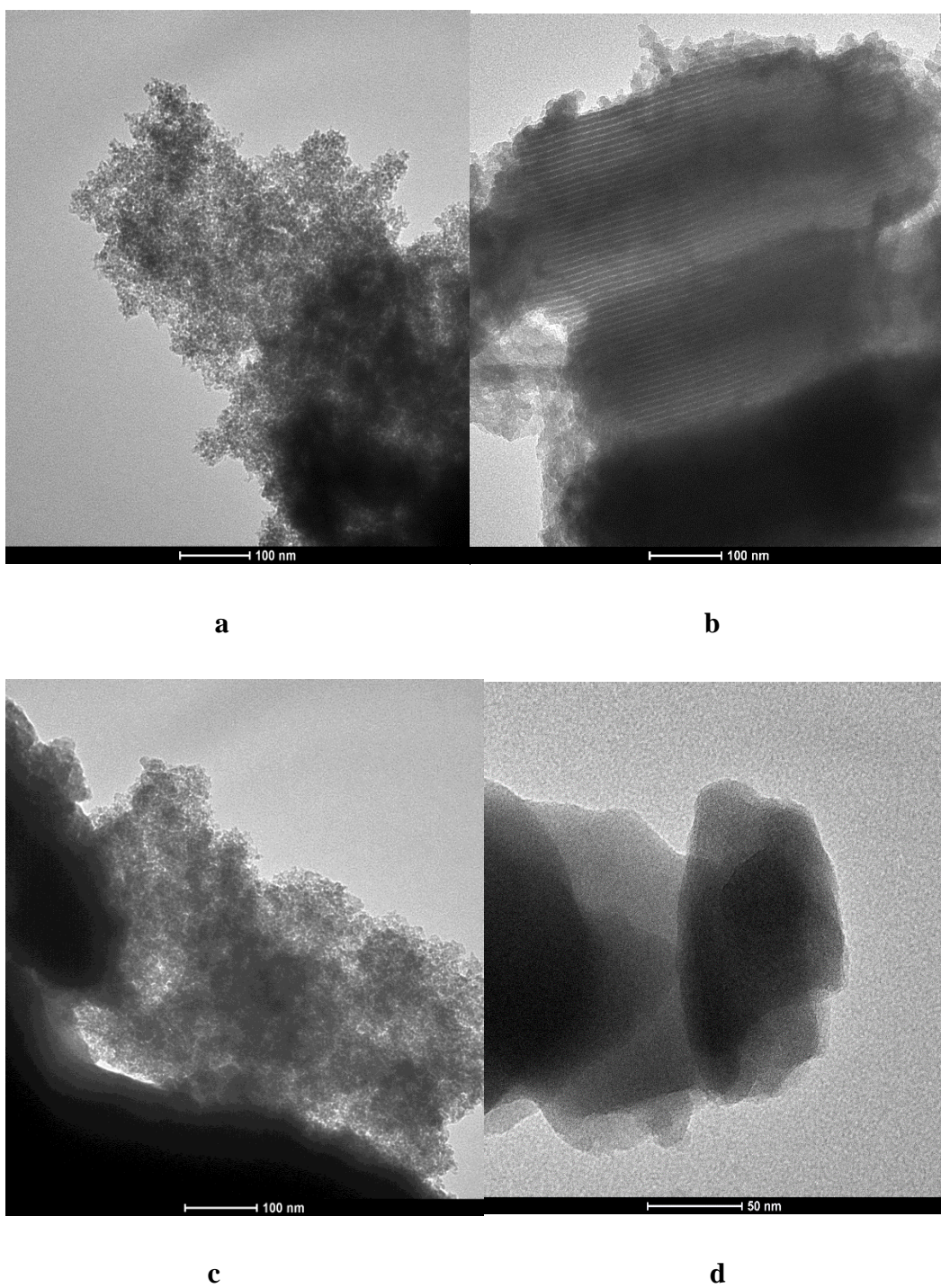
Figure 33 TEM images of a) SBA-15-B (100 nm), b) SBA-15-B@Clx$_{eth}$ (100 nm), c) SBA-15-B@Clx$_{meth}$ (100 nm), d) SBA-15-B@Clx$_{hex}$ (50 nm).

6.8 SCANNING ELECTRON MICROSCOPY (SEM) ANALYSIS

Morphology of silica samples was determined by scanning electron microscopy (SEM) in which SBA-15 appeared to have a rod-like shape (Figure 34, 35, and 36).

The SBA-15@Clx$_{eth}$ and SBA-15@Clx$_{meth}$ samples, while retaining the rod like shape, appeared to be elongated. In addition, from Figure 34, it can be observed that SBA-15@Clx$_{eth}$ had more particle size uniformity than the other samples. Crystallinity of Celecoxib loaded SBA-15 particles increases from methanol to hexane solvent. SBA-15@Clx$_{hex}$, however had disordered shape when compared with SBA-15@Clx$_{eth}$ and SBA-15@Clx$_{meth}$ (Figure 34-b).

a

b

c

d
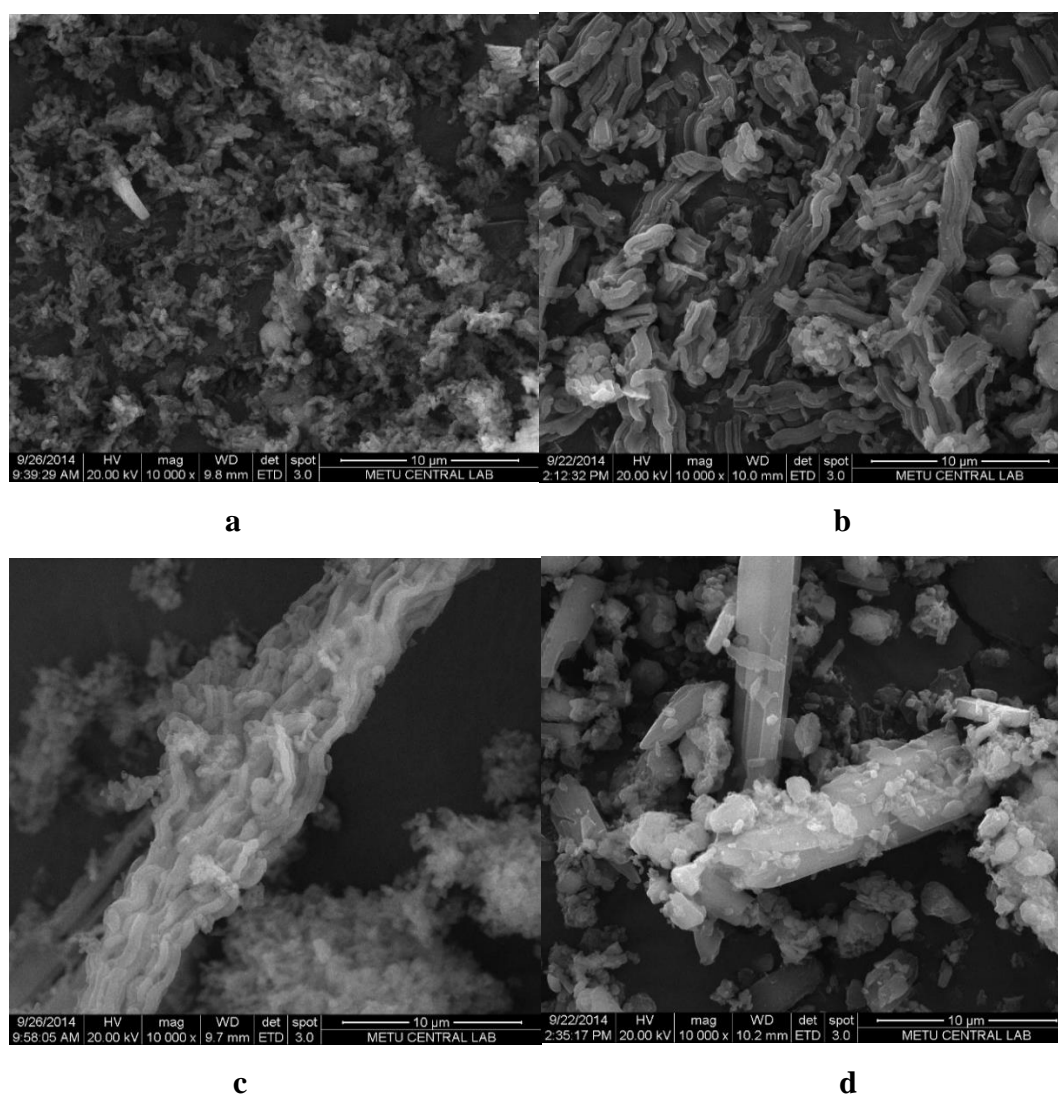
Figure 34 SEM images of a) SBA-15, b) SBA-15@Clx$_{eth}$, c) SBA-15@Clx$_{meth}$, d) SBA-15@Clx$_{hex}$.
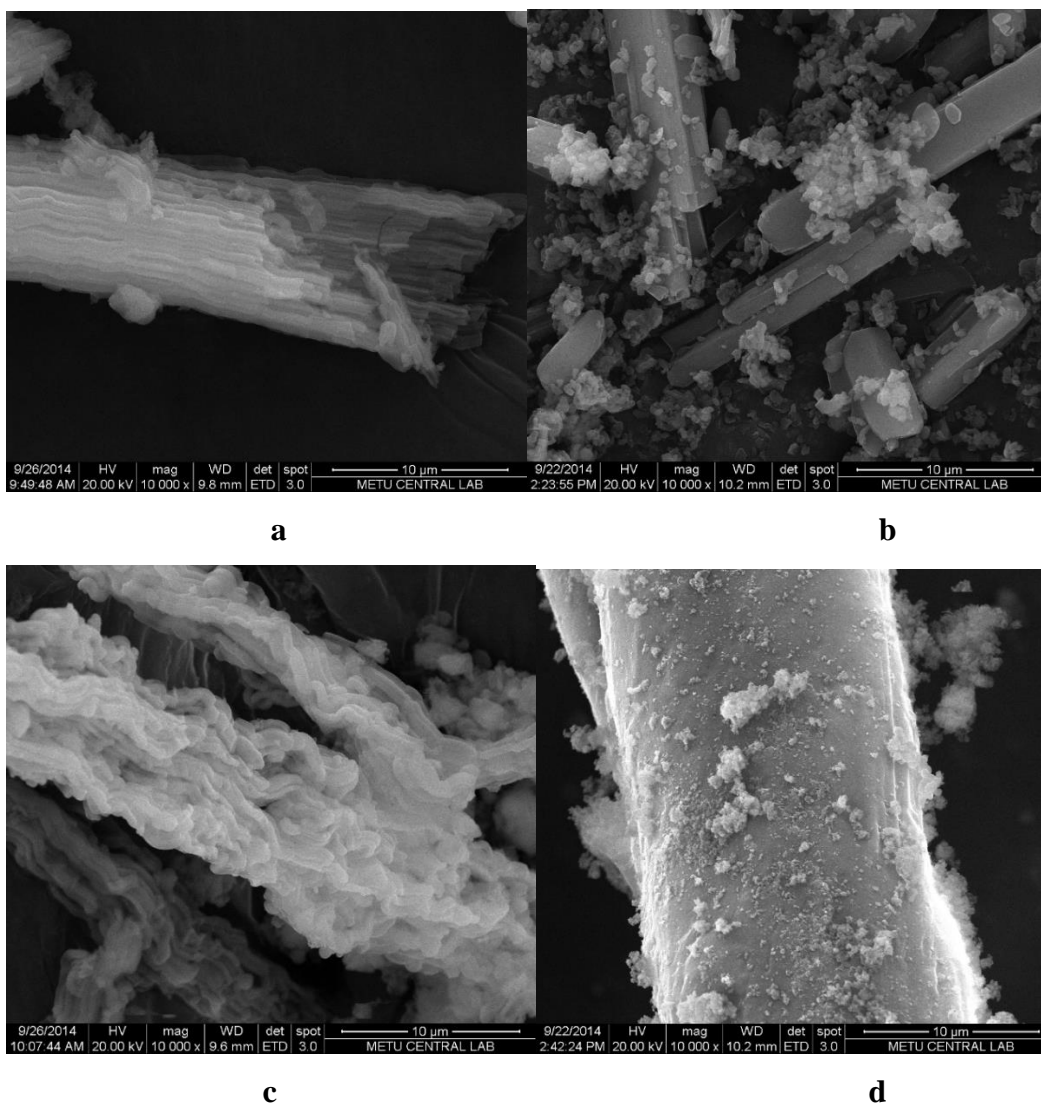
Figure 35 SEM images of a) SBA-15-A, b) SBA-15-A@Clx$_{eth}$, c) SBA-15-A@Clx$_{meth}$, d) SBA-15-A@Clx$_{hex}$.

After aminopropyl functionalization and drug loading, SBA-15-A@Clx$_{eth}$, SBA-15-A@Clx$_{meth}$ and SBA-15-A@Clx$_{hex}$ maintained their structural properties. Figure 35 shows a longer rod like shape of SBA-15-A with some crystalline forms of Celecoxib still remaining. The long rod like shape was also seen for SBA-15-A@Clx$_{meth}$; it is likely that in these samples Celecoxib was settled into the mesoporous channels, since no peak for crystalline Celecoxib was observed in powder XRD. In Figure 36-d, a change in the morphology of SBA-15-A@Clx$_{hex}$ was observed, most likely because of the solvent hexane.

a

b

c

d
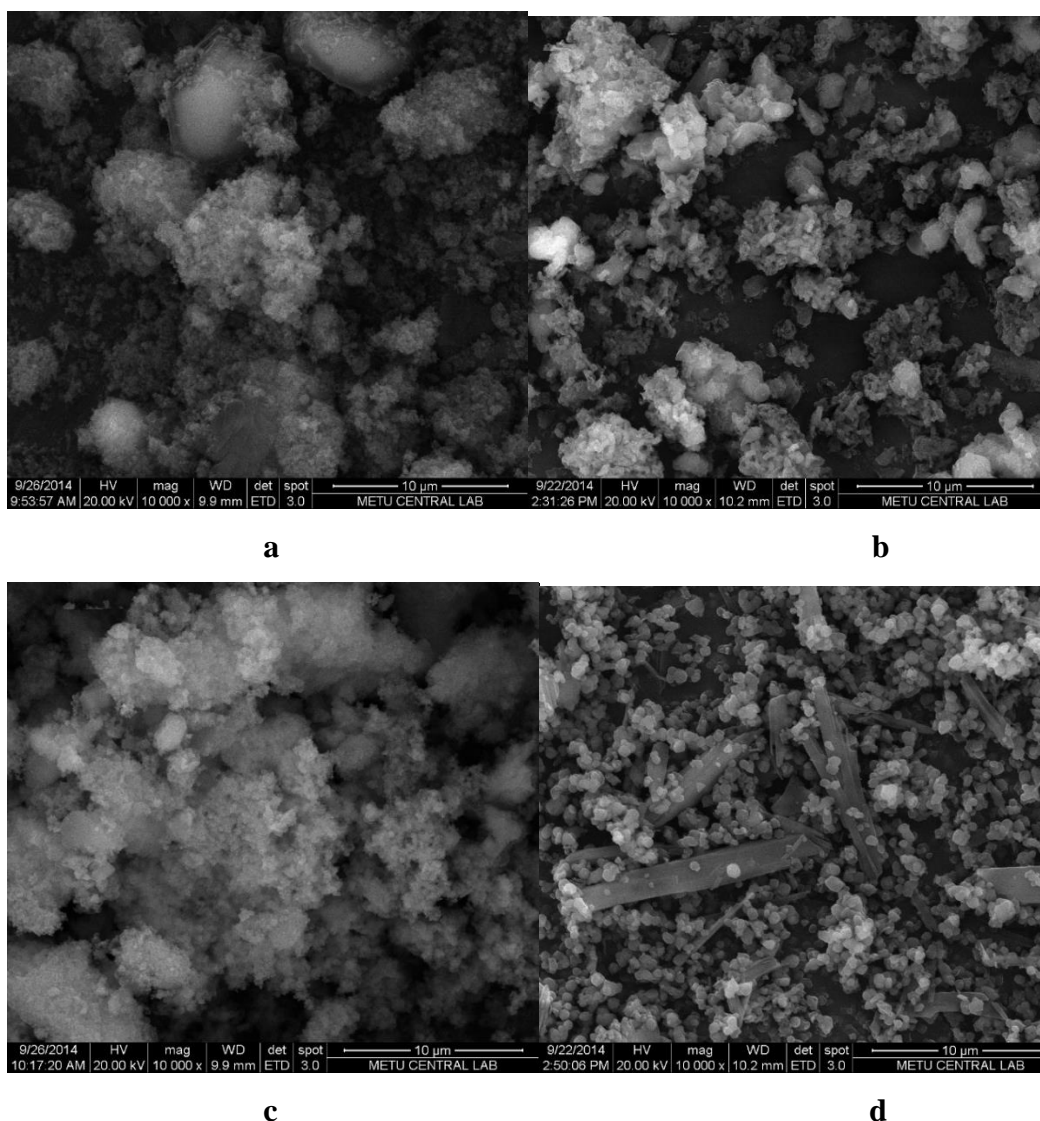
Figure 36 SEM images of a) SBA-15-B, b) SBA-15-B@Clx$_{eth}$, c) SBA-15-B@Clx$_{meth}$, d) SBA-15-B@Clx$_{hex}$.

In the SEM images of SBA-15-B particles, narrower pore sizes can be observed. Morphology for these borosilicate particles is different from the others, they are tiny spherical units. As seen in Figure 36-a, SBA-15-B had a disordered spherical shape; the particles were much smaller when ethanol was used as a solvent. Based on the data obtained from powder XRD and DSC, it may be concluded that Celecoxib mostly settled inside mesoporous channels of SBA-15-B@Clx$_{eth}$ (Figure 36-b). In Figure 36-c, a change of Celecoxib from crystal to amorphous phase can be clearly observed, further supporting the data obtained from powder XRD. In Figure 36-d, there are large

rectangular crystals inside small spherical silica particles as impurity that identified as undissolved drug crystals.

6.9 UV-VIS ANALYSIS

6.9.1 CELECOXIB LOADING

A standard curve for calibration was generated by measuring the UV-vis absorption of Celecoxib at the following concentrations: 0.003125 M, 0.00625 M, 0.0125 M, and 0.025 M. Celecoxib loaded silica samples (0.1 g) were dissolved in separate 50 ml of ethanol, methanol or hexane solvents. Obtained mixture was stirred for one day at ambient temperature, then prepared for UV analysis. The percentage of loaded Celecoxib was calculated with Beer's Law (A=ϵ.b.c) equation at 254 nm. In that equation, molar absorptivity is equal to the slope of calibration curve. Calibration curve's equation for loading process of Celecoxib in ethanol was obtained as y=0.0078x+0.0205 (R^2=0.8958). Calibration curves of loading process of Celecoxib in ethanol, methanol and hexane are seen in the Figure 37, Figure 38 and Figure 39, respectively.
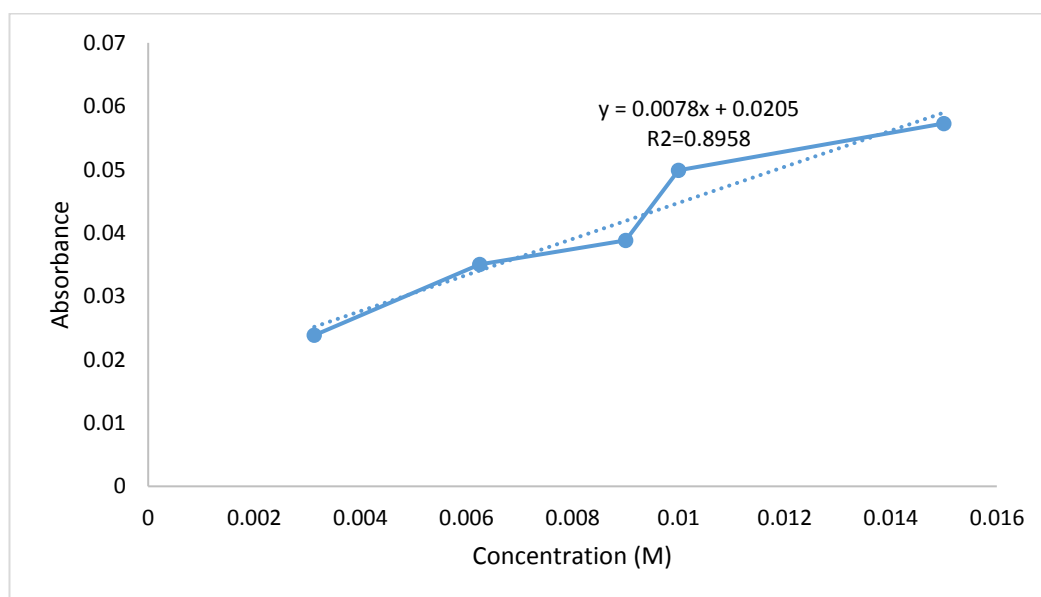
Figure 37 Calibration curve of loading process of Celecoxib in ethanol.
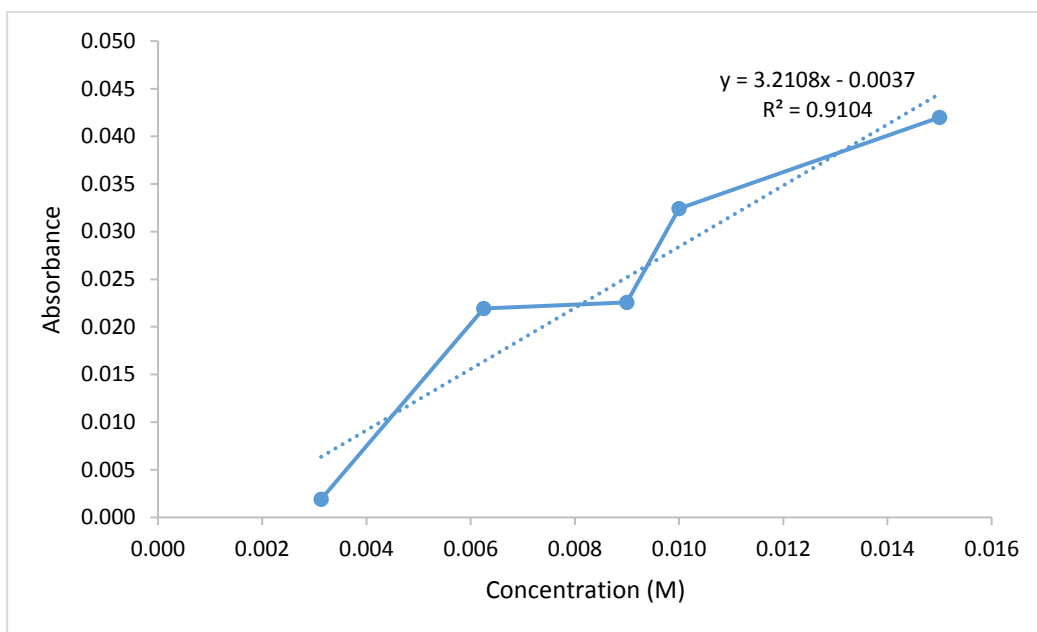
Figure 38 Calibration curve of loading process of Celecoxib in methanol.
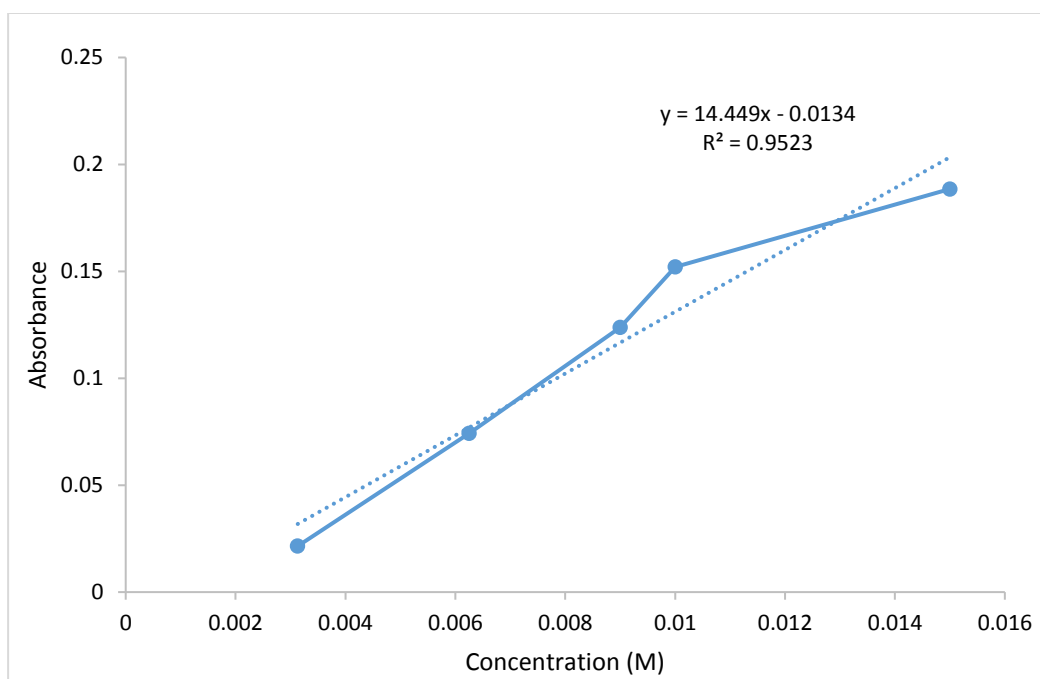
Figure 39 Calibration curve of loading process of Celecoxib in hexane.

Table 7 Celecoxib loading values with UV analysis and TGA analysis

Sample	(%) UV Analysis	(%) TGA Analysis
SBA-15@Clx$_{eth}$	25	25.3
SBA-15@Clx$_{meth}$	9	10.5
SBA-15@Clx$_{hex}$	**55**	**55.0**
SBA-15-A@Clx$_{eth}$	12	12.5
SBA-15-A@Clx$_{meth}$	6	7.10
SBA-15-A@Clx$_{hex}$	**32**	**32.9**
SBA-15-B@Clx$_{eth}$	23	23.0
SBA-15-B@Clx$_{meth}$	12	8.00
SBA-15-B@Clx$_{hex}$	**52**	**50.0**

Celecoxib loading values with UV analysis and TGA analysis are given in Table 7. Drug loading results of UV and TGA support to each other. According to the results, highest drug loadings were reached for Celecoxib loaded SBA-15 and SBA-15-B in hexane solvent. Amine functionalization of silica surface may limit the interaction of surface and drug molecules as well as drug loading capacity. In addition, the amount of Celecoxib loaded in SBA-15 particles was not affected by their morphology and pore diameter (Table 6 and Table 7). Although SBA-15-B@Clx$_{hex}$ had the lowest pore diameter, it showed the highest drug loading. Physical adsorptions like hydrogen bonding and electrostatic interactions between drug and the silica particles are important to ensure strong drug-support interactions. For SBA-15-B samples, the presence of -OH groups made the surface highly negative which may have enhanced the drug loading capacity. However, SBA-15-A had a positively charged surface due to the presence of aminopropyl groups on the surface; therefore, Celecoxib loaded SBA-15-A particles prepared in ethanol and methanol showed relatively lower drug loading. The reason of low drug loading in these particles can be also explained by strong polar solvent interactions with the surface of the particles.

Methanol and ethanol are polar solvents that have higher solubility parameters [60]. The solubility parameters of ethanol and hexane are 12.92 and 7.24, respectively. Celecoxib has amine and trifluoromethyl groups that are capable of forming hydrogen

bonds. Drug loaded silica samples prepared in ethanol and methanol showed lower drug loading than silica samples prepared in hexane. SBA-15@Clx$_{hex}$ and SBA-15-B@Clx$_{hex}$ had the highest drug loading, this was most likely because nonpolar hexane did not compete with the highly hydrophobic drug molecule hence, and drug loading was significantly increased. Celecoxib showed high affinity for ethanol and methanol, therefore the drug diffused much more in these solvents and accumulated in an amorphous form inside the pores of the silica particles. However, Celecoxib showed a lower affinity for hexane, which provided for high amounts of drug loading in crystalline form in SBA-15-B@Clx$_{hex}$ without good dispersion. This may also have resulted from unchanged pore diameter of SBA-15-B@Clx$_{hex}$ after the loading of Celecoxib. Moreover, isotherm type and hysteresis loop shape of this silica sample remained almost unchanged [52]. To conclude, high drug loading was achieved in Celecoxib loaded silica samples in hexane, however methanol and ethanol provided for a more uniform drug dispersion inside the pores in some cases.

6.9.2 CELECOXIB RELEASE

Release experiments were done as the same as loading process in phosphate buffer solution (PBS) at 37 ˚C at two different pH values, 7.4 and 5.0. 5 mL solvent was used to prepare of standard solutions in various concentrations of 0.003125 M, 0.00625 M, 0.0125 M, and 0.025 M. The measurements were recorded in the 200-800 nm range. Calibration curve's equation for release process of Celecoxib in PBS at pH=7.4 was obtained as y=27.3x+0.27, and at pH=5.0 was obtained as y=47.578x+0.2415. These calibration curves are seen in the Figure 40 and Figure 41.

For release process, 0.1 g Celecoxib loaded samples in ethanol, methanol and hexane were dissolved in 10 ml of PBS at pH=7.4 and pH=5.0 at 37 ˚C. The obtained samples were washed and filtered for UV analysis. All concentration measurements were recorded at 254 nm within 30 minutes, 1 hour, 2 hours, 4 hours, 6 hours, 24 hours and 72 hours. In order to calculate released drug amount, Beer's Law equation was used. In vitro release behavior of each of the mesoporous silica formulations were compared to commercial Celebrex. The release of Celecoxib from SBA-15, SBA-15-A and SBA-15-B was studied at pH 7.4 and 5.0, since cumulative release can be pH dependent.

Silica and drug crystallinity, surface are of silica and hydrophilic-hydrophobic inter-actions between silica and the drug could be important factors for release behavior [53].
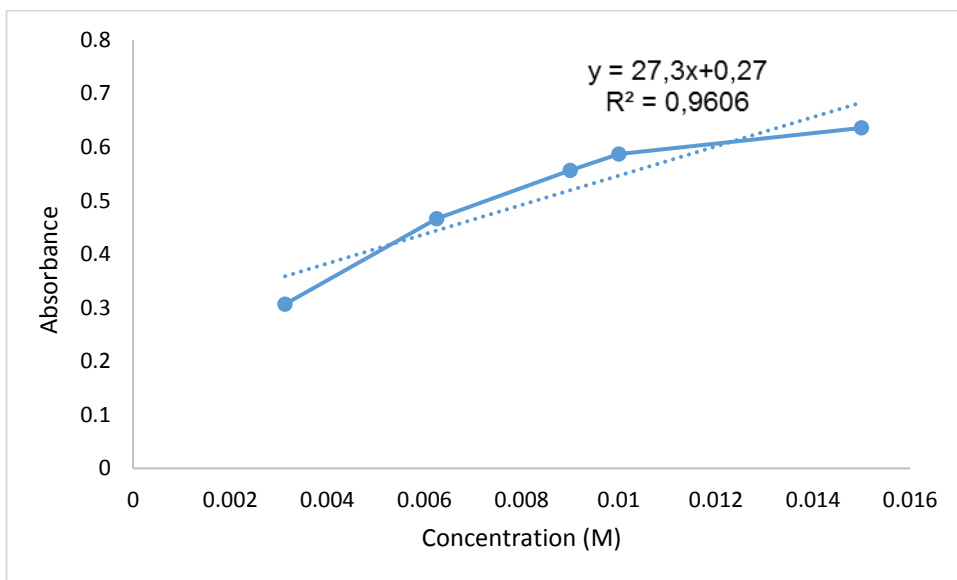
Figure 40 Calibration curve of release process of Celecoxib in PBS at pH=7.4.
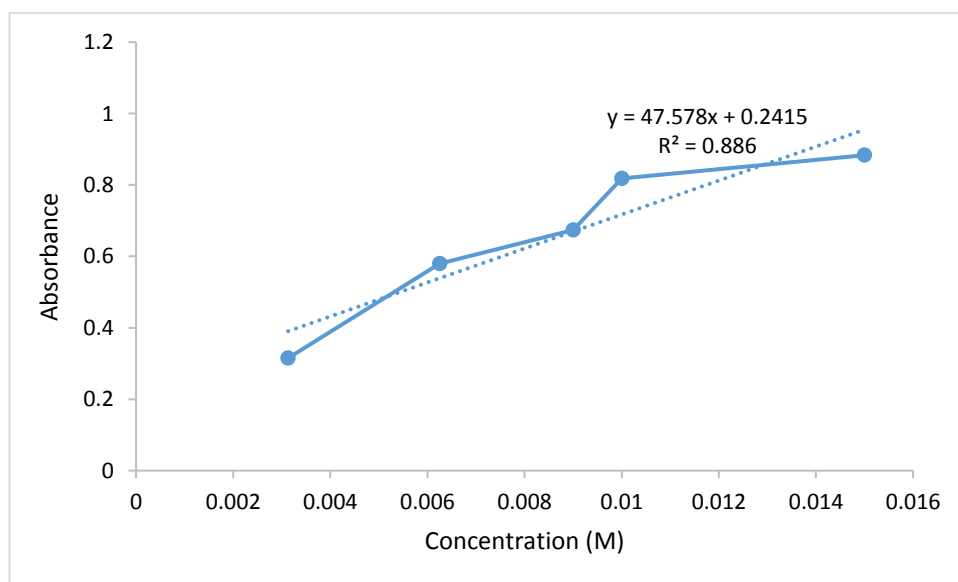
Figure 41 Calibration curve of release process of Celecoxib in PBS at pH=5.0.

Figure 42 Amount of Celecoxib released from 1.0 g of Celebrex loaded to SBA-15, SBA-15-A and SBA-15-B in ethanol in 72 hours at pH=7.4.

At pH=7.4 and pH=5.0, the release graphs of silica samples were seen between Figure 42-47. According to Figure 42, SBA-15@Clx$_{eth}$ and SBA-15-B@Clx$_{eth}$ reached highest drug release amounts. It may be concluded that release amounts of the Celecoxib were enhanced with using Celecoxib loaded mesoporous silica samples in ethanol solvent while Celebrex showed the lowest release amount.

SBA-15@Clx$_{eth}$ would allow more drug to be released and dissolved in the release medium. The burst drug release observed with SBA-15@Clx$_{hex}$, SBA-15@Clx$_{eth}$, SBA-15-B@Clx$_{eth}$, and SBA-15-B@Clx$_{hex}$ therefore may be related to the non-uniform filling of the pores with the drug. It is possible that a slower drug release may be observed if the pores could be filled more uniformly.

In Figure 43, all three Celecoxib loaded silica samples in methanol solvent showed slower release. SBA-15-A@Clx$_{meth}$ had nearly the same release curve with Celebrex

and had slower release behavior when compared to SBA-15@Clx_meth and SBA-15-B@Clx_meth. There is no big difference in release amounts between SBA-15@Clx_meth and SBA-15-B@Clx_meth. In the comparison between Figure 42 and Figure 43, sustained releases were observed for all samples in Figure 43, which could be very useful for controlled drug delivery. Moreover, functionalization and interaction of drug with low surface hydrophobicity of the silica are other indicative factors for drug release behavior. Organic functional group such as amines can reduce the hydrophobicity of silica surface, so slower diffusion and slower release could be observed.
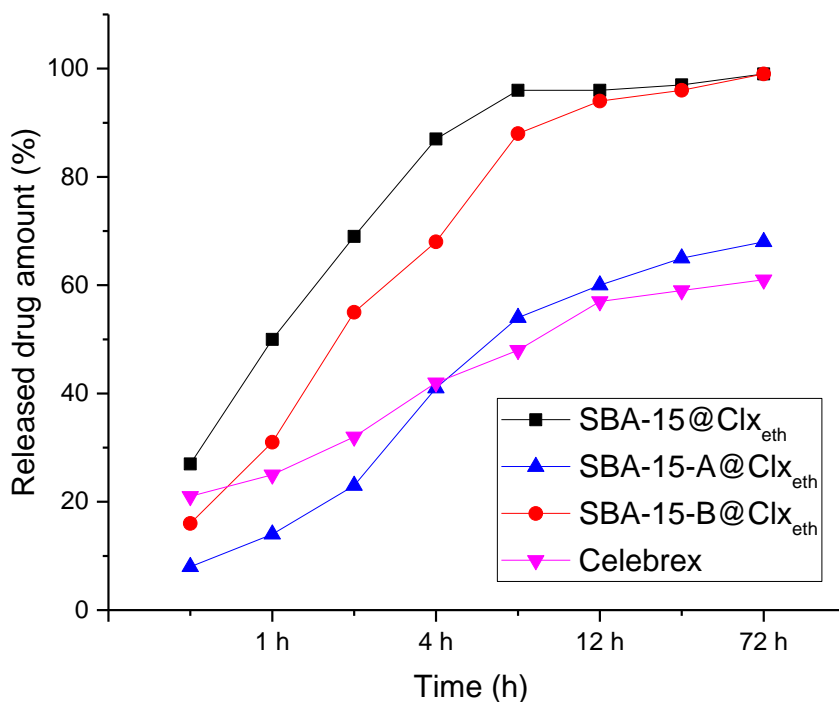

Figure 43 Amount of Celecoxib released from 1.0 g of Celebrex loaded to SBA-15, SBA-15-A and SBA-15-B in methanol in 72 hours at pH=7.4.

In Figure 44, the improvement of dissolution behavior and high release amount could be seen. This change may be as a result of increase in degree of Celecoxib crystallization. Because drug molecules accumulated on the outer pores of silica in hexane move firstly and regular diffusion of Celecoxib into the silica pores was not observed in silica samples prepared in hexane [53]. SBA-15-B@Clx_hex particles showed a burst type of

release, most likely since Celecoxib may be accumulated on the surface of SBA-15-B mesoporous silica. The surface adsorbed Celecoxib was released rapidly within 30 minutes. Furthermore, the interaction between silica and Celecoxib was very weak in the SBA-15-B particles due to the negative surface of borosilicate, which may have enhanced the solubility and release of the drug. Moreover, SBA-15-B had smaller particle sizes which may have resulted in faster drug release compared to the other silica samples. Drug release from larger sized particles generally take longer time since the drug is required to diffuse from inner pores to the release medium [61].

SBA-15 samples had higher pore volumes, and the release of Celecoxib from these samples was consistently higher compared to SBA-15-A since the larger pore volumes.
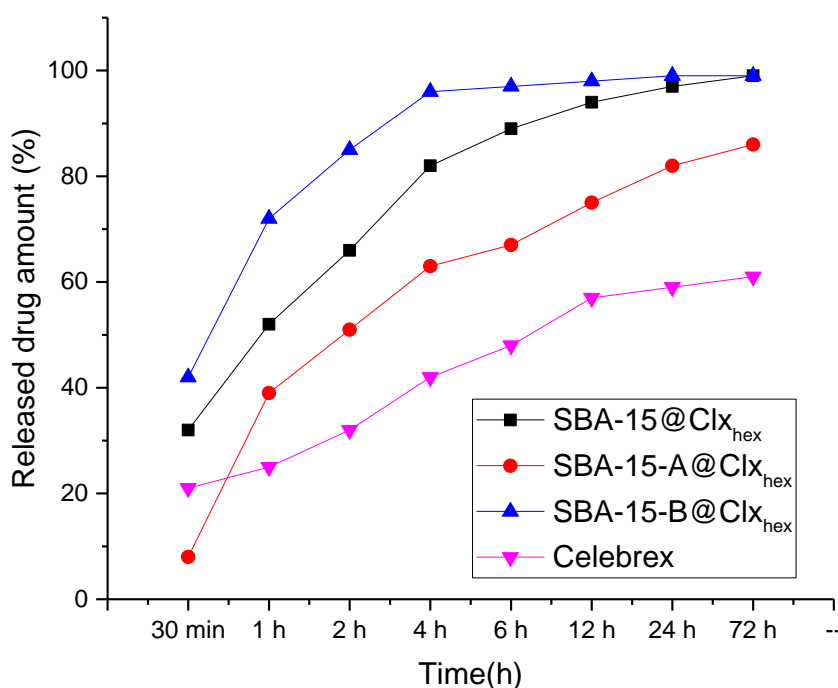
Figure 44 Amount of Celecoxib released from 1.0 g of Celebrex loaded to SBA-15, SBA-15-A and SBA-15-B in hexane in 72 hours at pH=7.4.
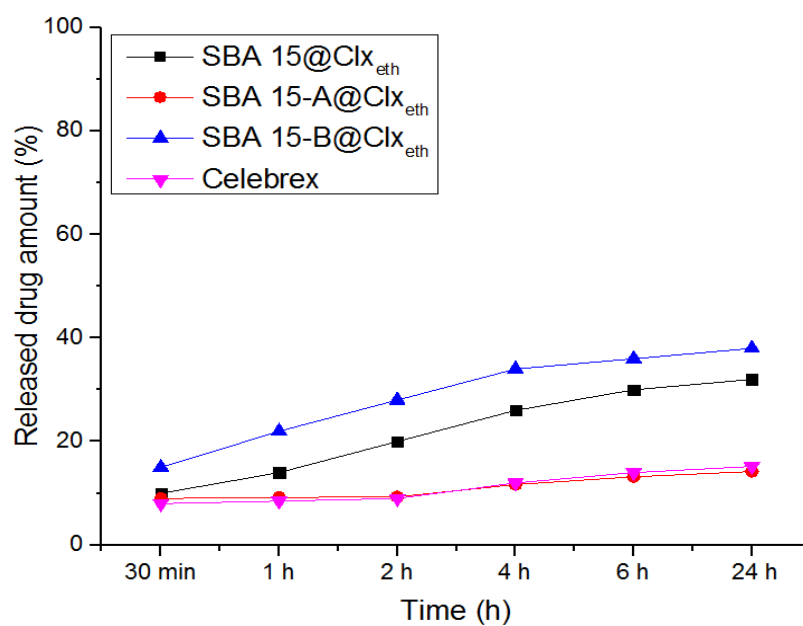
Figure 45 Amount of Celecoxib released from 1.0 g of Celebrex loaded to SBA-15, SBA-15-A and SBA-15-B in ethanol in 24 hours at pH=5.0.
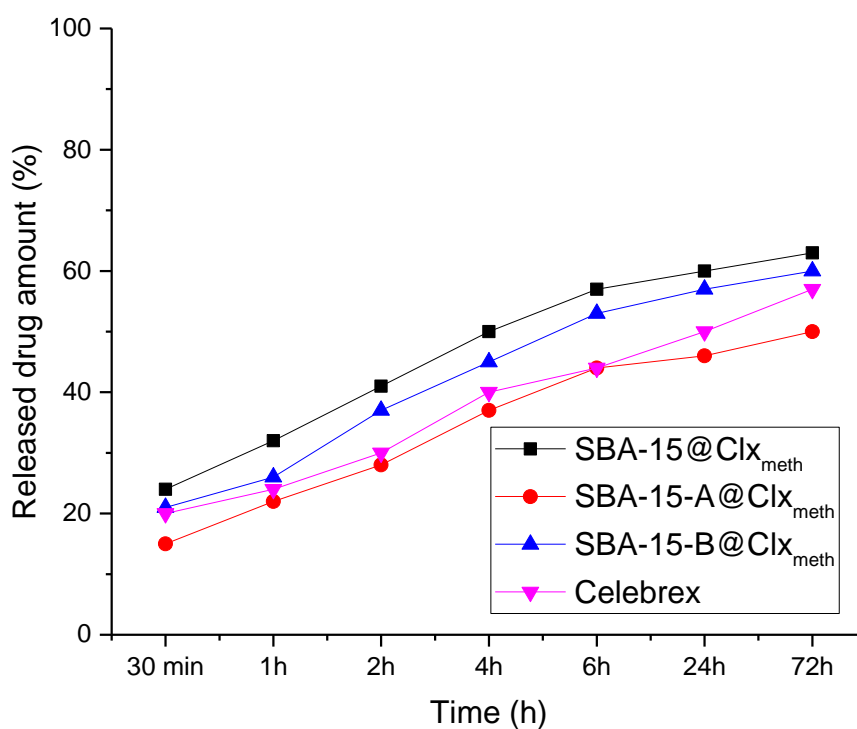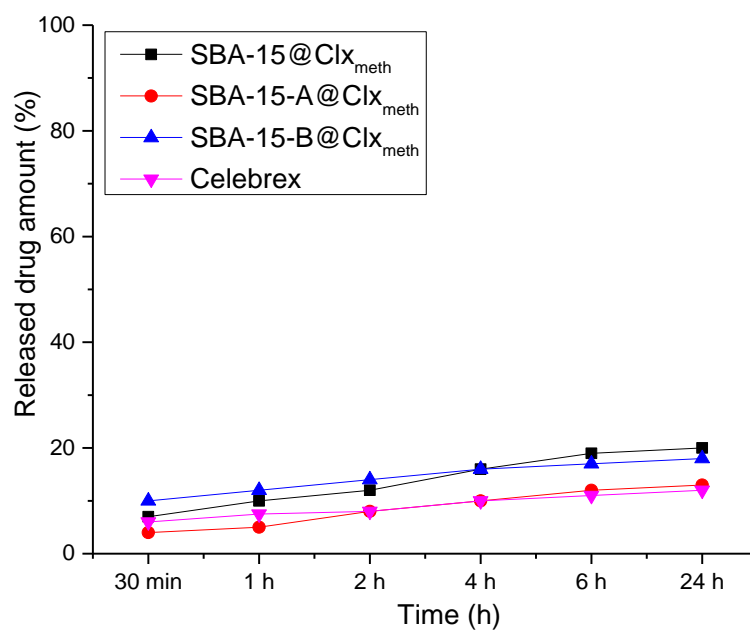

Figure 46 Amount of Celecoxib released from 1.0 g of Celebrex loaded to SBA-15, SBA-15-A and SBA-15-B in methanol in 24 hours at pH=5.0.
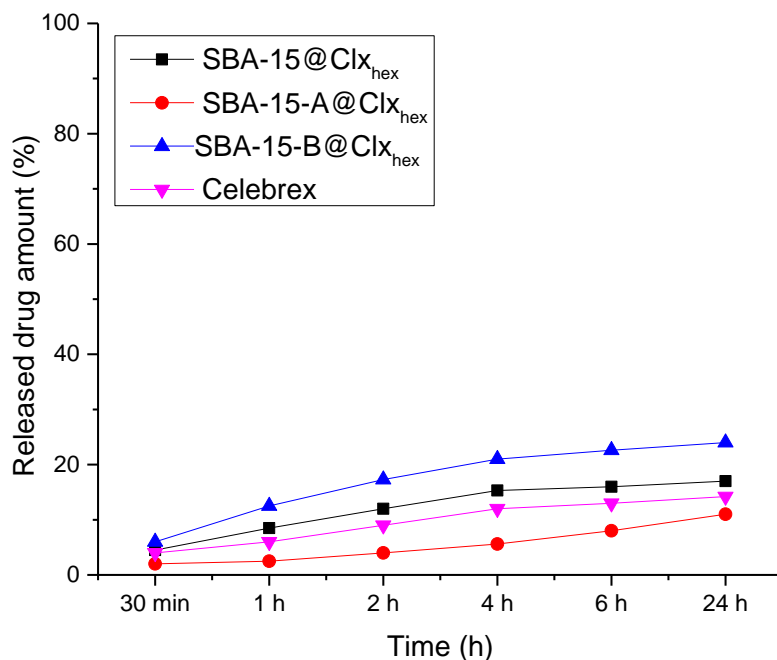
Figure 47 Amount of Celecoxib released from 1.0 g of Celebrex loaded to SBA-15, SBA-15-A and SBA-15-B in hexane in 24 hours at pH=5.0.

Figure 45, 46 and 47 show the amount of Celecoxib released from drug loaded silica samples at pH=5.0. The release rates have decreased within 24 hours for all three different Celecoxib loaded samples in ethanol, methanol and hexane at pH=5.0 when compared to pH=7.4. The release trend is very low in acidic environment, this is a result of acidic nature of Celecoxib and Celecoxib is more soluble at alkaline pH than acidic pH, which have 0.1192 and 0.1412 solubility values, respectively [62].

CHAPTER 7

7. CONCLUSION

In this study, SBA-15 mesoporous silica, APTES grafted SBA-15-A and boron doped SBA-15-B particles were examined as potential drug delivery agents for Celecoxib, a poorly water soluble drug with low bioavailability. Pure, functionalized and Celecoxib loaded in three different solvents silica samples were characterized for their physico-chemical properties.

The major findings of this study are as follows: 1. The loading capacity of Celecoxib in silica samples varied according to the type of solvent used and surface functionalization; release of the drug was also influenced by the solvent that the drug was loaded in and the pH. The amounts of Celecoxib loaded into SBA-15 particles having different pore diameters, pore volumes and surface charges, were increased when the non-polar solvent hexane was used. The highest drug loading capacity was found for SBA-15@Clx$_{hex}$ as % 55. The lowest drug loading capacity was observed in SBA-15@Clx$_{meth}$ with % 5.7 value. 2. Powder XRD patterns and DSC results showed that Celecoxib preserved its crystalline form in silica particles when the loading solvent was hexane. 3. TEM and SEM images indicated that hexane changed the morphology of silica samples; however, the release trend was nearly the same for drug loaded silica samples irrespective of whether ethanol, methanol or hexane were used as solvents. 4. Maximum drug loading and a burst release were observed in SBA-15@Clx$_{hex}$ and SBA-15-B@Clx$_{hex}$. The pH, crystallinity of the drug, surface potential of silica samples and the solvent that the drug was loaded in affected the release of Celecoxib from mesoporous silica samples. In conclusion, synthesized silica supports which have different particles sizes, pore volumes and functionalized groups on the surface could enhance solubility and bioavailability of Celecoxib and can be examined further for delivery of poorly water soluble drugs.

REFERENCES

1. Nowack, B.; Bucheli, T.D., "Occurence, behavior and effects of nanoparticles in the environment," *Environmental Pollution*, vol. 150, pp. 5-22., 2007.

2. Liu, J.; Bu, W.; Pan, L.; Shi, J., "NIR-Triggered Anticancer Drug Delivery by Upconverting Nanoparticles with Integrated Azobenzene-Modified Mesoporous Silica," *Angew. Chem. Int. Ed.*, vol. 52, pp. 4375-4379, 2013.

3. Colilla, M.; Gonzalez, B.; Vallet-Regi, M., "Mesoporous silica nanoparticles for the design of smart delivery nanodevices," *Biomater. Sci.*, vol. 1, pp. 114-134, 2013.

4. Kalbasi R. J., Zirakbash, A., "Synthesis, characterization and drug release studies of poly(2-hydroxyethylmethacrylate) KIT-5 nanocomposite as an innovative organic-inorganic hybrid carrier system," *RSC Adv.*, vol. 5, pp. 12463-71, 2015.

5. Wilson, C.G.; Crowley, P.J. *Controlled Release in Oral Drug Delivery*, 1st edition, 2011.

6. Romero, P.G.; Sanchez, C., "Hybrid Materials, Functional Applications. An Introduction," *Functional Hybrid Mater.* 2004.

7. Hashemikia, S.; Hemmatinejad, N.; Ahmadi, E.; Montazer, M. J., "Teracyline-Containing MCM-41 Mesoporous Silica Nanoparticles for the Treatment E.coli," *Colloid and Interface Sci.*, vol. 443, pp. 105-114, 2015.

8. Xu, R.; Pang, W.; Huo, Q. *Modern Inorganic Synthetic Chemistry*, p. 610, 2012.

9. "Representation of pore arrangement of ordered SBA-15 silica material", retrieved from http://nano.uib.no/abstracts/kleitz.html.

10. Schumacher K.; Ravikovitch P.I.; Du Chesne A.; Neimark A.V.; Unger K.K., "Characterization of MCM-48 Materials," *Langmuir*, vol. 16, pp. 4648-4654, 2000.

11. "Cubic unit cell of pore MCM-48" retrieved from http://www.patentbuddy.com/Patent/6096288.

12. Madan, R.D.; Prakash, S. *Modern Inorganic Chemistry*, p. 1576, 1987.

13. Vadia, N.; Rajput, S., "Mesopous Material, MCM-41: A New Drug Carrier," *Asian J. Pharm. Clin Res.*, vol. 4, no. 2 , pp. 44-53, 2011.

14. "Representation of MCM-41 and MCM-50" retrieved from http://www.mdpi.com/1996-1944/5/12/2874/htm.

15. Zhang, J.; Luz, Z.; Goldfarb, D., "EPR studies of the formation mechanism of the mesoporous materials MCM-41 and MCM-50," *J. Phys. Chem B* 101, pp. 7087-7094, 1997.

16. Moritz, M.; Geszke-Moritz, M., "Mesoporous materials as multifunctional tools in biosciences: Principles and applications," *Materials Science and Engineering C*, vol. 49, pp. 114-151, 2015.

17. Lu, J., Liong, M., Zink, J.I., Tamanoi, F., "Mesoporous Silica Nanoparticles as a Delivery System for Hydrophobic Anticancer Drugs," *General Nanotecnology : Small* vol.3, no. 8, 2007.

18. Kalhor, M.; Dadras, A.; Mobinikhaledi, A.; Tajık, H., "A New Method For One-Pot Synthesis of Aryloxyphenoxpropionate Herbicides Using 2,4,6-Trichloro-1,3,5-Triazine and (Bu)$_4$NI as a Homogeneous Catalyst," *J. Chil. Chem. Soc.,* vol. 56, no. 4, 2011.

19. Liberman, A.; Mendez, N.; Trogler, W.C.; Kummel, A.C., "Synthesis and surface functionalization of silica nanoparticles for nanomedicine," *Surface Science Reports,* vol. 69, pp. 132-158, 2014.

20. Slowing, I.I.; Vivero-Escoto, J.L.; Trewyn, B.G.; Lin, V.S-Y, "Mesoporous silica nanoparticles: structural design and applications," *J. Mater. Chem*, vol. 20, pp. 7924-7937, 2010.

21. Lim, M.H., Stein, A.: "Comparative studies of grafting and direct syntheses of inorganic-organic hybrid mesoporous materials.," *Chem. Mater.* vol. 11, 3285–3295 (1999).

22. Garcia, N.; Benito, E.; Guzman, J.; Tiemblo, P.; Morales, V.; Garcia, R.A., "Functionalization of SBA-15 by an Acid-Catalyzed Approach. A Surface Characterization Study," *Microporous and Mesoporous Mater.*, vol. 106, pp. 129-139, 2007.

23. Hwang, G.; Jeong, H.; Kim, Y., "Physical Properties of Barrier Ribs of Plasma Display Panels: I, Formation of Pores during Sintering of Lead Borosilicate Glass Frits," *J. Am. Ceram. Soc.*, vol. 85, pp. 2956-60, 2002.

24. Hwang, G.; Jeong, H.; Kim, Y., "Physical Properties of Barrier Ribs of Plasma Display Panels: I, Formation of Pores during Sintering of Lead Borosilicate Glass Frits," *J. Am. Ceram. Soc.*, vol. 85, pp. 2956-60, 2002.

25. Kshirsagar, N.A., "Drug Delivery Systems," *Indian Journal of Pharmacology*, vol. 32, pp. 554-561, 2000.

26. Perrie, Y.; Rades, T. *Pharmaceutics:Drug Delivery and Targeting*, 2nd edition, 2009.

27. Yang, P.; Quan, Z.; Li, C.; Lian, H.; Huang, S.; Lin, J., "Fabrication, characterization of spherical $CaWO_4$:Ln @MCM-41(Ln=Eu^{3+}, Dy^{3+}, Sm^{3+},Er^{3+}) composites and their applications as drug release systems," *Microporous and Mesoporous Mater.*, vol. 116, pp. 524-531, 2008.

28. Vallet-Regi, M.; Balas, F.; Arcos, D., "Mesoporous Materials for Drug Delivery," *Angew. Chem. Int. Ed.*, vol. 46, pp. 7548-7558, 2007.

29. Sharma, P.K.; Kumar, A., "Development, characterization and evaluation of Celecoxib micro emulsion for topical delivery," *J. Dispersion Sci. Tech.*, vol. 33, pp. 1411-1418, 2012.

30. Andersson J, Rosenholm J, Areva S, Lindén M. "Influences of material characteristics on ibuprofen drug loading and release profiles from ordered micro- and mesoporous silica matrices." *Chemistry of Materials.*, vol. 16, pp 4160–4167, 2004.

31. Song, S.W., Hidajat, K., Kawi, S., "Functionalized SBA-15 Materials as Carriers for Controlled Drug Delivery: Influence of Surface Properties on Matrix−Drug Interactions," *Langmuir,* 21, pp 9568-9575, 2005.

32. Kannao, S.U.; Bakade, B.V., "Solid Dispersion – A New Technique for Solubility Enhancement of Weakly Water Soluble Drug – A review," *IAJPR*, vol. 4, no. 6, pp. 2839-48, 2014.

33. Wischkel, C.; Schwendeman, S., "Principles of encapsulating hydrophobic drugs in PLA/PLGA microparticles," *Int. J. Pharmaceut*. 2008, 364, 298-327.

34. Savjani, K.T.; Gajjar, A.K.; Savjani, J.K., "Drug solubility: importance and enhancement techniques," *ISRN Pharmaceut.* 2012.

35. Liversidge, G.G.; Cundy, K.C., "Particle size reduction for improvement of oral bioavailability of hydrophobic drugs: I. Absolute oral bioavailability of nanocrystalline danazol in beagle dogs," *International Journal of Pharmecut.,* vol. 125, pp. 91-97, 1995.

36. Chaudhary, A.; Nagaich, U.; Gulati, N.; Sharma, V.; Khosa, V., "Enhancement of solubilization and bioavailability of poorly soluble drugs by physical and chemical modifications: A recent review," *J. Adv. Pharm. Edu.*, vol. 2, pp. 32-67, 2012.

37. Sekiguchi, K., & Obi, N. (1961). "Studies on absorption of eutectic mixture. I. A comparison of the behavior of eutectic mixture of sulfathiazole and that of ordinary sulfathiazole in man." *Chem. Pharm. Bull.,* 9, 866–872.

38. Serajuddin, A.T., "Solid dispersion of poorly water-soluble drugs: early promises, subsequent problems, and recent breakthroughs," *J. Pharmaceut. Sci.*, vol. 88, pp. 1058-1066, 1999.

39. Alvarez-Nunez, F.A., Yalkowski, S.H. "Relationship between polysorbate 80 solubilization descriptors and octanol-water partition coefficient of drugs",. *Int. J. Pharm.*, v.200, p.217-222, 2000.

40. Jambhrunkar, S.; Yu, M.; Yang, J.; Shotri, A.; Endo-Munoz, L.; Moreau, J.; Lu, G.; Yu, C., "Stepwise Pore Size Reduction of Oredered Nanoporous Silica Materials at Angstrom Precision," *J. Am. Chem. Soc.,* 2013.

41. Primo, F.T.; Froehlich, P.E., "Celecoxib Identification Methods," *Acta Farm. Bonaerense,* vol. 24, no. 3, pp. 421-5, 2005.

42. Sade, A., Tunçay, S.; Çimen, İ.; Severcan, F., Banerjee, S., "Celecoxib reduces fluidity and decreases metastatic potential of colon cancer cell lines irrespective of COX-2 expression," *Biosci. Rep.*, vol. 32, pp. 35-44, 2012.

43. "Structure of Celecoxib" retrieved from http://www.selleckchem.com/products/Celecoxib.html

44. Sevimli, F.; Yılmaz, A., "Surface functionalization of SBA-15 particles for amoxicillin delivery," *Microporous and Mesoporous Mater.*, vol. 158, pp. 281-291, 2012.

45. Chawla, G.; Gupta, P.; Tilagavathi, R.; Chakraborti, A.K.; Bansal, A.K. "Characterization of solid-state forms of celecoxib," *J. Pharmaceut. Sci.*, vol. 20, pp. 305-317, 2003.

46. Lee, K., Kang J. E., Park, S.K., Jin, Y., Chung, K.S., Kim, H.M., Lee, K., Kang, M. R., Lee, M. K., Song, K. B., Yang, E.G., Lee, J.J., Won, M., "LW6, a novel HIF-1 inhibitor, promotes proteasomal degradation of HIF-1α via upregulation of VHL in a colon cancer cell line," *Biochem. Pharmacol*, vol. 80, pp. 982-989, 2010.

47. Zhao, P.; Jiang, H.; Jiang, T.; Zhi, Z.; Wu, C.; Sun, C., Zhang, J., Wang, S., "Inclusion of celecoxib into fibrous ordered mesoporous carbon for enhanced oral bioavailability and reduced gastric irritancy," *European J. Pharmaceu. Sci*., vol. 45, pp. 639-647, 2012.

48. Salleh, N.F.M.; Jalil, A.A.; Triwahyono, S.; Nordin, S.N.; Kamarudin, N.H.N.; Effendi, J., "Amine modified mesostructured silica nano particles enhanced adsorption of phenol," *Jurnal Teknologi*, vol. 75, no. 6, pp. 1-6, 2015.

49. Glatter, O.; Kratky. O. *In Small Angle X-ray Scattering* London: Academic Pres, London, 1982.

50. Khodakov, A.Y.; Zholobenko, V.L.; I.-Clerc, M.; Durand. D., "Impact of Aqueous Impregnation on the Long-Range Ordering and Mesoporous Structure of Cobalt Containing MCM-41 and SBA-15 Materials," *J. Phys. Chem. B,* vol. 109, pp. 22780-22790, 2005.

51. Kang, T.; Park, Y.; Choi, K.; Lee, J. S.; Yi, J., "Ordered mesoporous silica (SBA-15) derivatized with imidazole-containing functionalities as a selective adsorbent of precious metal ions," *J. Mater. Chem.*, vol. 14, pp. 1043-1049, 2004.

52. Shang, F.; Wu, S.; Guan, J.; Sun, J.; Liu, H.; Wang, C.; Kan, Q., "A comparative study of aminopropyl-functionalized SBA-15 prepared by grafting in different solvents," *Reac Kinet Mech Cat*, vol. 103, pp. 181-190, 2011.

53. Zhu, W.; Wan, L.; Zhang, C.; Gao,Y.; Zheng, X.; Jiang, T.; Wang, S., "Exploitation of 3D face-centered cubic mesoporous silica as a carrier for a poorly water soluble drug: Influence of pore size on release rate,," *Materials Science and Engineering C*, vol. 34, pp. 78-85, 2014.

54. Nieto, A.; Balas, F.; Colilla, M.; Manzano, M.; Vallet-Regi, M., "Functionalization degree of SBA-15 as key factor to modulate sodium alendronate dosage," *Microporous and Mesoporous Mater.*, vol. 116, pp. 4-13, 2008.

55. Thielemann, J. P.; Girgsdies, F.; Schlolg, R.; Hess C., "Pore structure and surface area of silica SBA-15: Influence of washing and scale-up," *Beilstein Journal of Nanotechnology*, vol. 2, pp. 110-118, 2011.

56. Halamova, D.; Badanicova, M.; Zelenak, V.; Gondova, T.; Vainio, U., "Naproxen Drug Delivery Using Periodic Mesoporous Silica SBA-15," *Applied Surface Science*, vol. 256, pp. 6489-94, 2010.

57. Paul, M.; Pal, N.; Bhaumik, A., "Development and evaluation of novel solid nanodispersion system for oral delivery of poorly water-soluble drugs," *Materials Science and Engineering C*, vol. 32, pp. 1461-68, 2012.

58. Bahrami, Z.; Badiei, A.; Atyabi, F.; Darabi, H.R.; Mehravi, B., "thiol-functionalized mesoporous silica as nanocarriers for anticancer drug delivery," *Materials Science and Engineering C*, vol. 49, pp. 66-74, 2015.

59. Paulson, S. K.; Vaughn, M.B.; Jessen, S.M.; Lawal, Y.; Gresk, C. J.; Yan, B.; Maziasz, T. J.; Cook, C.S. A., "Pharmacokinetics of celecoxib after oral administration in dogs and humans; effect of food and site of absorption," *J Pharmacol Exp Ther*, vol. 297, no. 2, pp. 638-45, 2001.

60. Günaydın, Ş.; Yılmaz, A., "Inclusion of Celecoxib in MCM-41 Mesoporous Silica: Drug Loading and Release Property," *Turk. J. Chem.*, vol. 39, no. 2, pp. 1-17, 2014.

61. Liu, Y.; Sun, C.; Hao, Y.; Jiang, T.; Zheng, L.; Wang, S. J., "Dissolution and Bioa-vailability of drug from solid dosage form," *Pharm. Pharmaceut. Sci.*, vol. 13, pp. 589–606, 2010.

62. Agrawal, S.; Soni, N.; Jain, N.K.; Agrawal, G.P., "Solubility Enhancement of Poorly Water Soluble Celecoxib for Parenteral Formulations," *UPSR*, vol. 3, no. 7, pp. 2325-2336, 2012.